

A. Dugeai, Y. Mauffrey,  
A. Placzek, S. Verley  
(ONERA)

E-mail: alain.dugeai@onera.fr

DOI: 10.12762/2018.AL14-03

## Overview of the Aeroelastic Capabilities of the *e/sA* Solver within the Context of Aeronautical Engines

This paper presents the status of current development and research activities conducted at ONERA concerning the numerical modelling of aeroelastic phenomena of rotating machines. Three different topics are detailed after a short reminder of some features of ONERA's CFD solver *e/sA*. The first one addresses the development of methodologies for taking into account geometrical non-linear structural behavior in the modelling of the static aeroelasticity of large fan blades. The second one presents the current capabilities available for aeroelastic stability analyses of rotating machines conducted within the frame of stage and multi-stage configurations. The third point concerns the resolution of aeroelastic forced response problems. An overview of recent applications in the field of turbomachinery aeroelasticity will finally be drawn before giving some perspectives of new activities.

### Introduction

The Aeroelasticity Modeling and Simulation research unit of ONERA develops and validates numerical methods for the prediction of the aeroelastic behavior of aeronautical structures. This activity covers various applicative purposes, such as military and civil aircraft, aeronautical engines, and helicopters. This paper presents recent developments and applications conducted at ONERA, related to the prediction of the aeroelastic behavior of aeronautical rotating machines, such as fans, contra-fans, and open-rotors.

Over the last decades, a great effort has been made by several academic teams in the development of numerical methods for modelling the unsteady aerodynamics generated by fan blades vibrations, for the purpose of the prediction of dynamic aeroelastic stability (flutter) and forced response. Due to the complexity of unsteady flows occurring in industrial turbomachines, including compressibility, turbulence and separation effects in a large region of the operating domains, as well as rotor-stator interaction effects, aeroelastic stability in the field of turbomachines was studied using simplified formulations, such as linearized potential flow [1]. In the 90s, linearized Euler and Navier-Stokes formulations were then developed [2, 3, 4, 5] for the resolution of time-harmonic unsteady aerodynamic problems, introducing new numerical prediction methods for transonic flows in cascades. Since then, sector reduction techniques have been developed, assuming space-time periodicity properties in order to improve efficiency and face large 3D problems [6, 7, 8, 9, 10, 11, 12].

With increasing computational power, non-linear Euler and Navier-Stokes equations formulations in the time domain, including mesh deformation algorithms, have been also evaluated and developed since the mid-90s [13, 14, 15, 16, 17, 18, 19]. More recently, vibration problems have been addressed using a non-linear aeroelastic approach implementing a harmonic balance formulation. In this approach, the non-linear response of the fluid is modeled using a Fourier decomposition in the time domain of the periodic flow response to vibration [20, 21, 22, 23, 24].

The development of these unsteady aerodynamic numerical tools, using decoupled or fully coupled time-marching methods, has been a key player in the study of aeroelastic phenomena like stall and acoustic flutter [25, 26, 27], or flutter in the presence of distortion [28, 29] with applications to low-speed fans [30] and counter-rotating open rotor CROR [31, 32], as well as for the investigation of the forced-response phenomenon induced by blade passage effects in single-stage [19, 33] or multi-stage configurations [34, 35] and, more recently, by inlet distortion effects [36, 37, 29, 38]. Recent investigations have also been carried out to study the impact of structural non-linearities on the static aeroelastic behavior of large fan blades. Due to the dimension increase of fan and propeller blades for efficiency purposes, non-linear effects are indeed more likely to impact deformations and, in particular, centrifugal following forces have to be taken into account for the proper evaluation of hot blade shapes [39, 40].

All of these efforts contribute to the improvement of engine design, in order to face the current environmental challenges. In the trend of global reduction of the impact of aeronautical systems on the environment, very stringent constraints are indeed placed on Aircraft and Engine manufacturers to meet ACARE 2020 objectives, in order to reduce noise emission and drastically improve energetic efficiency. Compared to the figures for 2005, the emission reduction target levels are as high as 50% for CO<sub>2</sub>, 80% for NO<sub>x</sub> and 50% in terms of noise emission. Within this context, the external dimensions of aeronautical engines are becoming larger and larger, in order to achieve higher bypass ratios and thus higher efficiencies. To this end, the blade radii of fans and openrotors are increasing and new materials like composites are being used, resulting in more flexible structures prone to aeroelastic phenomena.

These new requirements are leading to new challenges for the prediction of the aeroelastic behavior of fan blades, due to larger sizes and greater flexibilities. Consequently, a new need emerges on the one hand to take into account the non-linear modelling of the blade structure to surpass the classical linear blade structural models. On the other hand, the need for a better modelling of the complex turbomachinery environment for aeroelasticity arises, in particular when it comes to considering the effects induced by adjacent blade rows in (multi-)stage configurations involving unsteady coupled interactions due to rotation and vibration, which are neglected in isolated blade row models usually considered for flutter, although they can be significant [41, 42].

In this paper, a first section will be devoted to the presentation of some details concerning the aerodynamic and aeroelastic solver *e/sA*, developed by ONERA, which has been implemented in the presently discussed studies. A first point will focus on the coupling features developed within the aeroelastic module, in order to couple the aerodynamic solver *e/sA* with the structural solver MSC Nastran, enabling fully non-linear static aeroelastic simulations. Then, specific insight will be given into specific sector-reduction techniques used in the case of the aeroelastic modelling of turbomachines, implementing phase-lagged and multiple-frequency phase-lagged boundary conditions. Eventually, a discussion on available methods for forced response problems will be given. The last section of the paper will present some applications of these features and techniques.

## Aerodynamic Solver *e/sA*

The present work has been conducted with the *e/sA* solver, developed at ONERA (ONERA-Airbus-SAFRAN property). This project started in 1997 within ONERA's aerodynamics department, and is now being developed by a large number of contributors from several departments within ONERA, as well as by industrial or academic partners, such as AIRBUS, SAFRAN, CERFACS, ECL/LMFA and CENAERO. *e/sA* is a multipurpose aerodynamic software dedicated to the simulations of external and internal flows for aircraft, turbomachinery, helicopter and propellers, among other applications [43].

### *e/sA* Aerodynamic Solver Features

*e/sA* allows aerodynamic computations for compressible viscous and inviscid flows. It handles RANS and URANS equations with a large set of turbulence models, ranging from algebraic to turbulent transport equations, including Reynolds Stress Models, Detached or Large Eddy Simulation (DES, LES) models, which are now being implemented for some applications. Laminar-turbulent transition criteria

are also available, including the Menter transport equation model. Considering the meshing strategy, *e/sA* was initially developed as a multiblock structured grid solver. However, incoming developments have gradually been made to increase its capabilities, in order, first to take into account partially or non-coincident block joins, and then to handle Chimera overset grids. Patched grid and overset Chimera grid techniques can be implemented to overcome multiblock structured grid meshing issues for complex geometrical configurations. Moreover, hybrid structured/unstructured mesh capabilities are now available, which have been extensively validated in particular for taking into account turbomachinery complex geometries, including technological effects (cavities, injections, cooling devices, and trenches). The use of Cartesian grids is available.

Motion and deformations of bodies can be taken into account for steady/unsteady applications. The finite-volume approach is used for spatial discretization in connection with centered or upwind schemes (Jameson, Roe, Van Leer). High-order schemes are available or under development in *e/sA* (k-exact schemes), and Runge-Kutta or backward Euler time schemes are available. Local, global, dual and Gear time stepping schemes are implemented. Convergence can be accelerated using implicit techniques and/or multigrid resolution schemes. For unsteady time-accurate simulations, Dual Time Stepping and Gear schemes are available. For rotating machinery problems, relative frame with either relative or absolute variable formulations can be used for turbomachinery, helicopters and propellers. Parallelization is achieved through the distribution of mesh blocks over a set of processors. As far as unsteady computations are concerned, *e/sA* is able to handle mesh deformation using an Arbitrary Lagrangian Eulerian (ALE) formulation of flow equations.

### *e/sA/Ael* Aeroelastic Module

The Aeroelasticity Modelling and Simulation research unit of ONERA has been developing, within the *e/sA* solver, a specific module for solving aeroelastic problems, either static or dynamic. A general framework has been developed in the optional "Ael" module of *e/sA* over the last few years [44, 45, 46, 47], in order to extend *e/sA* to different kinds of static or unsteady aeroelastic simulations (Figure 1).

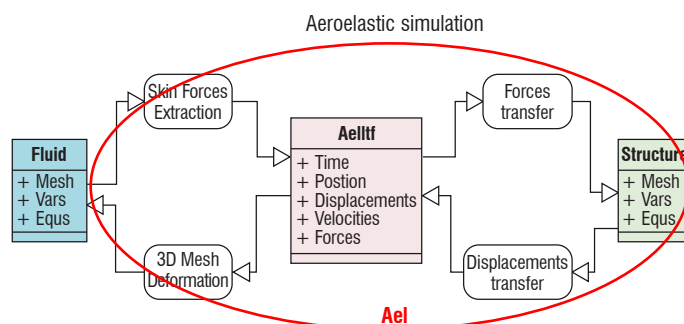


Figure 1 – Connections between the fluid and structural solver within the *e/sA/Ael* aeroelastic module

The purpose of these simulations is the prediction of the in-flight static or dynamic behavior of flexible aerodynamic structures and their aeroelastic stability. This "Ael" subsystem gives access, in a unified formulation, to different types of aeroelastic simulations, compatible with the flow solver features. The available simulations include non-linear and linearized harmonic forced motion computations, static coupling and consistent dynamic coupling simulations in

the time-domain. The harmonic balance method is also implemented for periodic forced motion simulations.

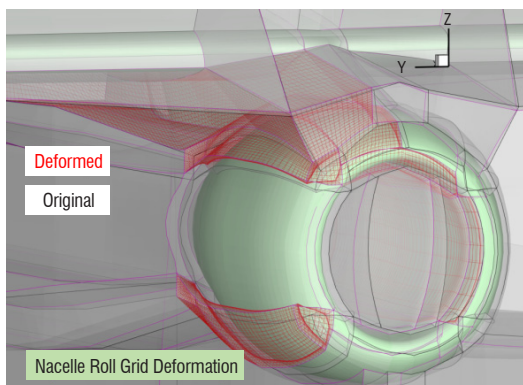
In the Ael module, however, only a simple linear structural behavior is assumed and implemented. Various kinds of linear structural modeling are available ("reduced flexibility matrix" for static coupling, modal approach, or full-finite-element structural model). In addition to the specific aeroelastic simulation driver, the *e/sA/Ael* module basically integrates three main subsystems: a module for data transfer between the fluid and structure solvers (including load and displacement components), an integrated static and dynamic linear structural solver and a 3D fluid mesh deformation tool.

Transfer of displacements and loads between the structure and the fluid are based on the exchange of generalized coordinates and forces in the case of the modal approach, whereas it uses specific interpolation or smoothing techniques, the nearest neighbor or virtual-work-principle-based techniques for the finite-element approach. With regard to the important issue of 3D fluid mesh deformation, several techniques are also implemented in the Ael module. A first technique is based on the resolution of an equivalent linear elastic continuous medium problem, whose boundary conditions prescribe the displacement of the aerodynamic grid at the aeroelastic interfaces. An 8-node hexahedral finite-element approach is used to discretize the aerodynamic grid mesh deformation problem. The local stiffness matrix is computed approximately, using a one-point Gauss integration procedure, specifically corrected for Hour-glass spurious mode treatment. The static equilibrium of the discretized system leads to the following linear system:

$$K_{ii}q_i = -K_{if}q_f \quad (1)$$

where  $K_{ii}$  and  $K_{if}$  are stiffness matrices resulting from the discretization of the structural analogy problem, and where  $q_i$  and  $q_f$  are respectively the computed and boundary prescribed displacement vectors. Given that the stiffness matrix is positive definite, the system is solved using a pre-conditioned conjugated gradient method. For *e/sA*, the technique is implemented in the case of multi-block structured grids. The full-mesh deformation is defined as a sequence of individual block deformations.

Boundary conditions are set to impose zero or prescribed displacement values, to move on a plane, on the local surface boundary, or along or normally to a prescribed vector, and to achieve deformation continuity through block interfaces. In order to fulfil the boundary conditions, the conjugated gradient algorithm is modified.



(a) oscillating nacelle

The resolution procedure is kept compatible with the boundary conditions by iteratively projecting the solution and search direction vectors in the proper linear subspace. However, performing structural static deformation computations on the full aerodynamic grid is expensive, and reduction techniques are implemented to solve the structural problem on a coarse grid, by packing cells, especially in the boundary layer regions, where the aerodynamic discretization is extremely dense.

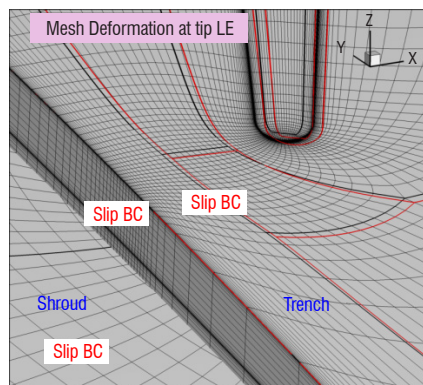
The structural analogy method is very versatile and is used for a wide range of applications, including turbomachines, aircrafts, helicopters, propellers and CRORs (see Figure 2). The mesh deformation procedure implemented has been validated for use with Chimera grids, and is now being fully parallelized in the current *e/sA* version.

An alternate mesh deformation method based on a mixture of the Inverse Distance Weighting (IDW) method and TransFinite Interpolation (TFI) is also available in the case of multiblock structured configurations. IDW is implemented in order to prescribe displacements on block boundaries, and the displacements of internal block nodes are obtained from the boundaries using the TFI algorithm. New developments are currently being made, in order to implement a Quaternion-based mesh deformation method in a robust and efficient way, using a Fast-Multipole Method accelerated IDW algorithm.

The time-consistent unsteady aeroelastic simulations discussed in this paper are performed using dual time stepping or Gear methods. These simulations allow for the evaluation of the aeroelastic stability of aeronautical structures, either in a weakly-coupled or strongly-coupled strategy. In the weak coupling case, the motion of the structural model is prescribed as a single harmonic motion, or a combination of harmonic motions, which can be rigid or can follow its natural vibration modes  $\Phi$ . The structure is indeed classically considered as a linear elastic medium for aeroelastic stability analyses and the structural displacement field  $x$  of the vibrating structure subjected to aerodynamic forces  $F_A$  satisfies the discretized equations of motion:

$$M\ddot{x} + D\dot{x} + Kx = F_A(x, t) \quad (2)$$

Assuming a linear behavior of the structural model, the displacement field is approximated as a linear combination of the first structural mode shapes  $x \approx \Phi q$  and the following reduced system is obtained after projection on the modal basis:



(b) axial compressor with trench clearance at shroud

Figure 2 – Mesh deformation examples using structural elastic analogy

$$\mu\ddot{q} + \beta\dot{q} + \gamma q = GAF(q, t) \quad (3)$$

where

$$\mu = \Phi^T M \Phi \quad \beta = \Phi^T D \Phi \quad \gamma = \Phi^T K \Phi \quad GAF(q, t) = \Phi^T F_A(x, t) \quad (4)$$

are respectively the generalized mass, damping and stiffness matrices and the generalized aerodynamic force. Weakly-coupled aeroelastic computations are run over several periods of vibration, in order to obtain the unsteady aerodynamic response to a forced motion of the structure prescribed with the modal shapes  $\Phi$ . The aerodynamic temporal response of the fluid gives access to unsteady pressure distributions on the model surface, and may be integrated to obtain unsteady aerodynamic loads over the structure. With the purpose of performing a linear stability analysis for flutter, these pressure load distributions  $F_A(t) = -pn$  are projected onto the structural modal basis shapes  $\Phi$ , to obtain the unsteady Generalized Aerodynamic Forces  $GAF(t) = \Phi^T F_A(t)$ , which are involved in the right hand side of the modal structural dynamics equation (3).

A first harmonic analysis of the unsteady forces is performed to study, in the frequency domain, the aeroelastic stability of the fluid-structure coupled system. Flutter response is classically analyzed using the  $p-k$  stability method [49], Karpel's minimum state smoothing method [50] or energy considerations [48].

In the strong coupling case, the structural dynamics equation is directly solved in the time domain during the unsteady aerodynamic computation, using a Newmark resolution scheme. At each physical time step, aerodynamic forces and elastic forces are balanced using an additional coupling loop, usually requiring 3 steps for the proper convergence of the fluid-structure equilibrium. The procedure then gives access to the unsteady evolutions of the structural variables, and of the aerodynamic field as well.

### Resolution of Static Aeroelastic Equilibrium within a Non-Linear structural Context

In many aeroelasticity problems, the structure can be classically assumed to behave linearly. However, in some cases, the linear

structure assumption is no longer valid. This is the case when geometric non-linearities, such as large displacements, are to be considered, for example for highly flexible wings, or in the turbomachine case, for rotating blades of large dimensions, such as large propellers, open-rotors or UHBR fan blades.

Therefore, new solutions for coupling non-linear aerodynamics and non-linear structural models are to be considered. The fluid-structure problem can be formulated as a coupled-field problem, where the solutions are coupled only at the boundary interfaces between the fluid and the structure [51]. It is then possible to run separate solvers for the flow computation and the structure computation, and to reach a coupled solution by exchanging information at the common fluid-structure boundaries.

The currently implemented mechanism used for coupling *elsA* and an external Computational Structural Mechanics (CSM) solver basically relies on the exchange of data at the aeroelastic interface, using a CGNS standard compliant interface. The aeroelastic module features of *elsA* are used, except for the internal structural model resolution, which is externalized. The standard aeroelastic simulation is interrupted at each coupling step, and aerodynamic forces relative to an embedded reduced structural model (either modal or finite element) are computed using the *elsA/Ael* aeroelastic module integrated force transfer methods. This data is extracted and provided to the CGNS memory database, which in turn is processed by an external Python coupling script in charge of the communication with the external structural solver. The CSM solver Nastran is run in non-linear mode with the dedicated SOL400 solution, taking into account the following forces for the prescription of aerodynamic forces at each time step. At the end of the structural solver step, displacements on the reduced structural model are sent back to *elsA* and transferred to the aeroelastic interface. 3D aerodynamic mesh deformation is then performed, before continuing with new fluid resolution iterations.

This architecture has been developed for the purpose of running aeroelastic simulations coupling *elsA* with the non-linear commercial structural solver MSC NASTRAN. To this end, a specific interface written in C language and based on the use of the OpenFSI module of Nastran has been developed and coupled with a Python interface (Figure 3).

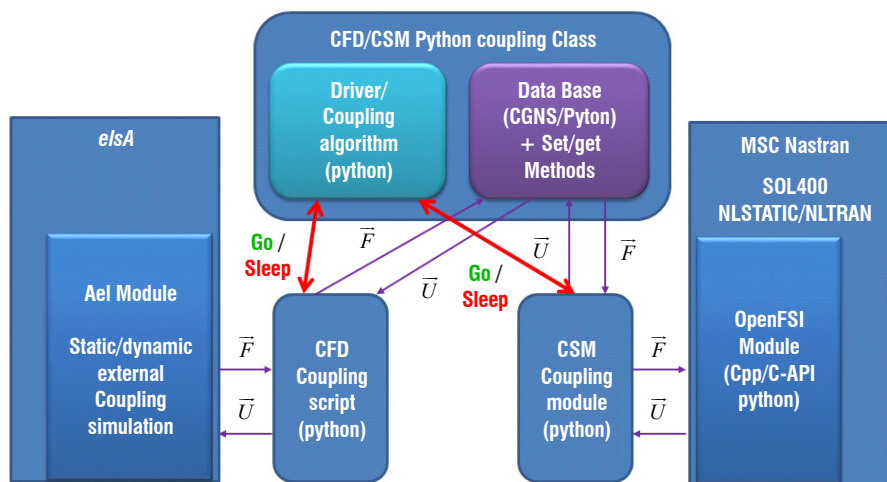
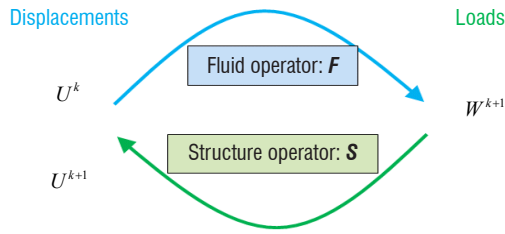


Figure 3 – Current coupling architecture between *elsA* aerodynamic solver and MSC Nastran SOL 400 non-linear structural solver



$$X^k = \begin{bmatrix} u^k \\ w^k \end{bmatrix}$$

$$X^{k+1} = \begin{bmatrix} u^{k+1} = S(w^{k+1}) \\ w^{k+1} = F(u^k) \end{bmatrix}$$

$$X^{k+1} = X^k + \alpha(SF(X^k) - X^k)$$

Figure 4 – Fluid-structure fixed-point algorithm

The coupling strategy is basically a fixed-point method, potentially requiring the use of a relaxation procedure to ensure convergence (Figure 4). This mechanism has been implemented in the case of static hot shape predictions of UHBR and open-rotor fan blades. In this case, the non-linear structural modelling is mandatory, due to effect of high-speed rotation inducing additional stiffness terms and centrifugal forces.

## Dynamic Aeroelasticity Features for Stage/Multistage Turbomachine Configurations

### Reductions for Dynamic Aeroelastic Stability Problems for Cyclic Periodic Configurations

The aeroelastic module of  $e/sA$  can be used for the study of the aeroelastic stability of aeronautical structures, using the weakly-coupled approach described previously. In this case harmonic forced motion simulations are performed, in order to obtain the generalized aerodynamic forces  $GAF(t)$  giving access to the aerodynamic damping.

The stability of an aeroelastic coupled system is analyzed from the behavior of the structural linear dynamic system governed by Equation 2 or by Equation 3, when the system is projected onto the structural mode shapes of interest. In this latter case, the knowledge of the generalized aerodynamic forces  $GAF(t)$  resulting from the projection of the aerodynamic forces  $F_A(x)$  onto the structural mode shapes is necessary to perform the stability analysis and weakly coupled simulations are run for that purpose.

The stability analysis is aimed at evaluating whether the coupling of the aerodynamic flow with the modal vibrations produces additional damping or amplification of the motion, which is likely to lead to the destruction of the structure, through the so-called flutter phenomenon. Consequently, the linear stability analysis of the modal equation (3) is performed, in order to seek complex exponential solutions of the system in the form

$$q(t) = q^* e^{pt} \quad \text{with} \quad p = j\omega(1 + j\alpha) \quad (5)$$

The solution may be damped or amplified, whether the real part of the eigenvalue  $p$  is negative or not.  $\omega$  is the pulsation and  $\alpha$  is the particular solution damping. Therefore, the substitution of the particular solution (5) in the structural dynamics equation (3) leads to:

$$(p^2 \mu + p\beta + \gamma)q^* e^{pt} = GAF(q, t) \quad (6)$$

Assuming then that the vibration-induced generalized aerodynamic forces are linear with respect to the structural motion (included in phase and out-of-phase components), leads to:

$$GAF(q, t) \approx Aq + B\dot{q} \quad (7)$$

Finally, the stability of the coupled system is conditioned by the eigenvalues of the homogeneous problem:

$$(p^2 \mu + p(\beta - B) + (\gamma - A))q^* = 0 \quad (8)$$

The aerodynamic stiffness  $A$  and damping  $B$  for the various mode shapes of interest are obtained via harmonic forced motion simulations, which lead to the identification of the generalized aerodynamic force matrix in the frequency domain. The stability of the system then depends solely on the value of the aerodynamic damping  $B$ .

In the case of perfectly tuned turbomachine configurations, the geometry and the mechanical solution fields are assumed to exhibit a cyclic symmetry periodicity. This property satisfied by the structural and aerodynamic flow fields allows for channel reduction formulations, which are described in the following subsections.

### Phase-Lagged Boundary Conditions

The phase-lagged boundary condition holds in the case of a single purely time-periodic phenomenon. This is basically the case in harmonic forced motion simulations implemented for the purpose of an aeroelastic stability analysis of a perfectly tuned isolated blade row, as described in the previous section.

In the case of cyclic symmetric structures, the deformation of the structure may be represented in the linear case as a combination of nodal diameter mode shapes, for which successive blades vibrate at a specific inter-blade phase angle. The vibration of the row can be described by the duplication of a reference sector, taking into account the phase shift induced by a specific inter-blade phase angle. This property allows for the single-sector reduction of the aeroelastic harmonic forced motion simulation, where only the reference sector is modeled. Specific boundary conditions at the limits of the computational domain are to be used to take into account a specific value of the inter-blade modal vibration phase-shift.

Due to the azimuthal periodicity of the deformation, a generic displacement field can be represented as a Fourier series in azimuth, and taking into account the cyclic symmetry of the row (made up of  $N$  identical sectors), it can be expressed as the sum of so-called diameter modes  $u_n$  as written below:

$$u(r, \theta, z, t) = \Re \left\{ \sum_{n=0}^{N-1} u_n(r, \theta, z, t) \right\} \quad (9)$$

Each nodal diameter component exhibits a boundary condition between the values of  $u_n$  at the upper and lower azimuthal boundaries

of the sector, associated with a specific value of inter blade phase angle  $\sigma_n$ , which can be expressed as follows:

$$u_n(r, \theta + \beta, z, t) = u_n(r, \theta, z, t) e^{i\sigma_n} \quad \text{with } \sigma_n = n\beta \quad (10)$$

where  $\beta = 2\pi / N$  is the azimuthal extension of the sector.

In the case of an aeroelastic simulation with a prescribed harmonic motion following an  $n$ -nodal diameter mode of vibration  $\Phi_n$  inheriting the same phase-shift property, the temporal evolution of the reference sector displacements can be expressed as:

$$u_n(r, \theta, z, t) = \Phi_n(r, \theta, z) q^* e^{i\omega t} \quad (11)$$

The phase-lagged boundary conditions (10) expressed with the phase angle  $\sigma_n$  can be reformulated for a harmonic motion, in such a way that the displacement fields on both azimuthal boundaries are connected by the time-shift of duration  $\tau = \sigma_n / \omega$ , corresponding to the propagation time of the deformation/unsteady flow component rotating wave through the sector boundaries:

$$\begin{aligned} u_n(r, \theta + \beta, z, t) &= \Phi_n(r, \theta, z) e^{i\omega t} e^{i\sigma_n} \\ &= \Phi_n(r, \theta, z) e^{i\omega \left( t + \frac{\sigma_n}{\omega} \right)} \\ &= u_n \left( r, \theta, z, t + \frac{\sigma_n}{\omega} \right) \end{aligned} \quad (12)$$

These properties extend to the flow field induced by the structural motion, which also exhibits the same  $n$ -nodal diameter azimuthal periodicity at the convergence of the process:

$$w_n(r, \theta + \beta, z, t) = w_n(r, \theta, z, t) e^{i\sigma_n} = w_n \left( r, \theta, z, t + \frac{\sigma_n}{\omega} \right) \quad (13)$$

This condition is implemented in *elsA* for aeroelastic simulations with a prescribed harmonic motion as the so-called "chorochronic" boundary condition, using a moving-average Fourier decomposition process in the time domain that is relevant because of the time-periodic features of the phenomenon. This Fourier analysis is conducted at each time step at upper and lower boundaries of the sector, and characteristic relations are used to establish the equilibrium with the flow reconstructed at a shifted time on the other boundary using the current Fourier coefficients [8] [10].

### Extension of the Phaselagged Boundary Conditions in the Case of Stage Aeroelastic Simulations

In the case of harmonic forced motion simulations conducted on a turbomachine stage configuration, two different periodic phenomena are superimposed. The first is the effect of a periodic blade passage of the opposite row, and the second is the rotating wave of deformation induced by the propagation wave of the considered  $n$ -nodal deformation mode shape. Since both phenomena are driven by non-commensurable fundamental frequencies in the general case, the resulting unsteady flow field is basically not periodic in time. Using an assumption of small perturbations, the unsteady flow field can be represented as a summation of rotating perturbation waves due to both phenomena. Following Tyler and Soffrin [52] and He [9], the unsteady flow can be approximated as:

$$w(r, \theta, z, t) \approx w_0(r, \theta, z) + \sum_{p=0}^{N_p-1} w_p(r, \theta, z, t) \quad (14)$$

where  $w_p$  is a rotating wave associated with a specific phenomenon, whose characteristics are a specific wave number  $\kappa_p$  (or nodal diameter) and a specific pulsation  $\omega_p$ . Each rotating wave exhibits a specific rotation speed  $c_p = \omega_p / \kappa_p$ , and phase-lagged boundary conditions like (10) can be applied at the upper and lower boundaries of the considered row sector distant from the sector angle  $\beta = 2\pi / N$ , with specific phase and/or time shift for each rotating wave, as described in Table 1 [53]. The same approximation based on the superposition principle can also be considered for multistage configurations [54] [12], in which case the rotating waves correspond to the blade passage effects of the two adjacent rows.

	Wave number	Pulsation	Phase shift	Time shift
	$\kappa_p$	$\omega_p$	$\sigma = \kappa_p \beta$	$\tau = \frac{\kappa_p}{\omega_p} \beta$
Blade passing	Number of opposite blades $N_{opp}$	Pulsation of blade passing $N_{opp} \Delta\Omega$	$N_{opp} \beta$	$\frac{\beta}{\Delta\Omega}$
Vibration	Nodal diameter $n$	Vibration pulsation $\omega$	$n\beta$	$\frac{n\beta}{\omega}$

Table 1 – Frequency-time relationships for a rotating wave component

The moving average Fourier decomposition/reconstruction process at the sector boundaries, as well as on the blade row stage interfaces, is applied here separately for each rotating wave component, in order to prescribe the proper boundary conditions. For better robustness, a relaxation procedure is applied at each time step on the Fourier coefficients of each rotating wave included in the simulation. These boundary conditions are implemented in the following unsteady simulations presented hereafter in the applicative section.

### Forced Response in the Turbomachinery Stage

Forced response is a dynamic aeroelastic phenomenon. It corresponds to the dynamic response of a structure due to impinging unsteady aerodynamic forces. Contrary to flutter, the excitation forces are assumed to be independent from the system vibration. However, the excitation forces induce vibration, which in turn adds vibration-induced aerodynamic forces. This phenomenon is likely to occur when upstream wakes are striking a downstream located structure, which is subject to unsteady aerodynamic forces, and therefore starts to vibrate. The level of vibration depends on the mechanical characteristics of the structure (in particular, structural damping) and on the amplitude and frequency of the excitation. This phenomenon can also arise in the case of external flows, for example, when an unsteady wake develops from the main wing surface to the horizontal tail plane of an aircraft, thus creating vibrations, or in the case of turbomachinery flows, where the excitation source may come from the upstream wakes of an adjacent blade row in (multi-)stage configurations or from non-uniformities in the inlet flow breathed by the engine, which can be induced by inlet geometry, a cross-wind generating flow separation or the ingestion of a boundary layer, for example.

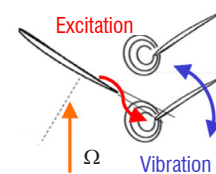


Figure 5 – Illustration of the load sources involved in the forced-response phenomenon for a rotor/stator stage.

## Forced Response in the Turbomachinery Stages

In the case of a turbomachinery engine stage, let us say for a rotor/stator configuration like the one described in Figure 5, the flow field of the rotor is seen at each rotation by the stator blades as an unsteady perturbation, due to the differential rotation between both row frames. This effect generates an excitation of the stator blades whose frequency is a multiple of the rotation speed. Potentially dangerous forced-response levels may occur when there is coincidence between the excitation frequency and the natural frequency of the excited system. When this frequency is close to one of the blade eigenmodes, the blade oscillates and the vibration amplitude may be large depending on the system damping. A high vibration level may lead to material fatigue, or even destruction of the blade row.

In the turbomachinery case, frequency coincidences are likely to occur between rotation speed harmonics and natural frequencies of the different mode shapes of the excited row, especially during low to high regime of rotation modifications for operating condition transitions of the engine (acceleration or deceleration). Therefore, the potential coincidences are usually plotted in the classical Campbell diagram, as shown by the intersections of curves in Figure 6.

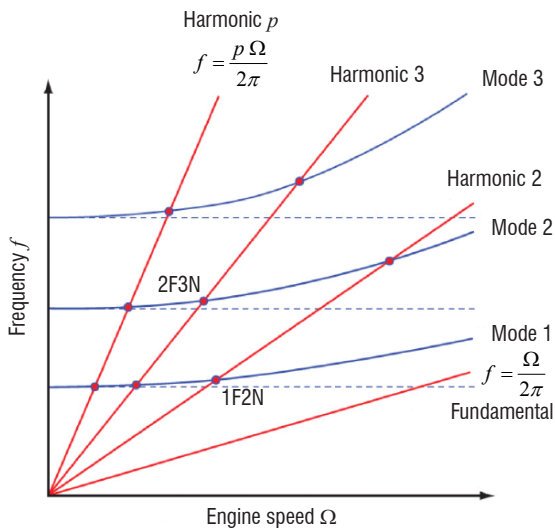


Figure 6 – Campbell diagram representing the structural mode frequencies as a function of the rotation speed in blue, and the different engine harmonics in red. Crossings between both types of curve may lead to a high level of vibration.

### Forced Response of a Linear Structure

As for the weakly-coupled aeroelastic simulations performed for flutter analyses, a linear elastic model of the structure can be considered and the projection of the dynamic equations of motion on the mode shapes of interest leads to the reduced system of Equation 3 already considered for flutter in the previous section. The analysis of the forced-response phenomenon is, however, different from that of the aeroelastic stability of the system, since the purpose is to study the system response to an excitation field, in order to find the amplitude and phase of the induced vibration. The aeroelastic forced response is due to the combination of two kinds of generalized aerodynamic forces  $GAF(t) = F_{exc}(t) + F_{vib}(t)$ :

- the excitation generalized force  $F_{exc}$  (assumed to be motion independent) due to an external force,

$$F_{exc}(t) = \Phi^T F_{Aexc}(t) \quad (15)$$

- the aeroelastic generalized force  $F_{vib}$  generated by the structure vibration due to the excitation,

$$F_{vib}(q, t) = \Phi^T F_{Avib}(x, t) \quad (16)$$

Under the assumption of force linear superposition, which is standard in classical linear aeroelasticity, the contribution due to the vibration  $F_{vib}$  can be approximated as in Equation 7 for flutter analysis, as:

$$F_{vib}(q, t) \approx Aq + B\dot{q} \quad (17)$$

Substituting the previous expression in the dynamic equation of motion (3) results in:

$$\mu\ddot{q} + (\beta - B)\dot{q} + (\gamma - A)q = F_{exc}(t) \quad (18)$$

The effect of the aerodynamic forces due to the vibration is double:

- Induce additional stiffness ( $A$  coefficient),
- Induce additional positive or negative damping ( $B$  coefficient).

This aerodynamic damping  $B$  is likely to influence the level of forced response of the system. As is well known, near resonance, the level of vibration of a linear structural dynamic system is, roughly speaking, inverse proportional to the damping coefficient. Therefore, in order to properly predict aeroelastic forced response levels, it is mandatory to correctly evaluate the total aeroelastic damping  $\beta - B$  and, consequently, of the aerodynamic damping  $B$ . The situation is all the more critical in the case of small values of the structural damping  $\beta$ , which may be small compared to aerodynamic damping  $B$ .

### Classical Numerical Approaches for the Resolution of Forced-Response Problems

Several numerical approaches are available for the resolution of aeroelastic forced response problems.

The first one is the classical linear superposition method. In this approach, both the excitation and vibration phenomena are handled separately. The corresponding aerodynamic forces  $F_{exc}$  and  $F_{vib}$  are then summed, following a linear superposition assumption whose relevance has been investigated [34] [55]. Therefore, two numerical simulations are performed, the first taking into account the excitation only (no vibration), and the second with vibration and no excitation. The vibration simulation gives access to the aerodynamic stiffness and damping, but a linear assumption is made. Moreover, no coupling between excitation and vibration can be represented. This time domain approach may be expensive, because two fully-converged simulations are necessary, but frequency-domain approaches can help to reduce these costs [34].

The second approach is the fully-coupled fluid/structure dynamic simulation [34] [35]. This brute force approach does not make any assumption of linearity or superposition. The fully-coupled fluid-structure system is solved in the time domain. Aerodynamic non-linearities are taken into account, and excitation and vibration forces are fully represented and coupled. However, for low damping values, the simulation may be very expensive, due to the large transient needed to reach the stabilized periodic solution, which is characteristic of the forced-response phenomenon.

The extension of the method to non-linear structures is not considered here, but may be addressed either in the case of local non-linearities using

the Craig and Bampton approach including additional degrees of freedom, and non-linear force terms or, in a more general framework, using specific methods for the resolution of the non-linear structural dynamics, such as the harmonic balance method for structures (see [56]).

### Twin Approach

A third approach has been proposed by Mesbah [57], and evaluated at ONERA [58], which is referred to as the twin approach. In this approach, both vibration and excitation phenomena are included in the same single simulation, which is the so-called "twin" simulation. No linearization of the aerodynamic forces (as in the decoupled approach) is introduced here, but there is no need to solve for a long transient either, until forced response levels convergence (as in the time domain coupled approach), which may be extremely expensive, especially for low damping values. Indeed, the simulation is not coupled in the sense that a forced vibration motion is prescribed at the excitation frequency and at a specific amplitude and phase angle with respect to the excitation. These amplitude and phase angles are tuned during the simulation, in order to reach the proper values matching the forced-response phenomenon. To this end, the equilibrium of the structural dynamic system (3) subject to the combined aerodynamic forces  $GAF(t) = F_{exc}(t) + F_{vib}(t)$  is solved and the characteristic of the (multi)harmonic motion is iteratively corrected until convergence.

The corresponding procedure is described as follows. At forced response, the aerodynamic forces and motion are periodic and the structural dynamics equations (3) are considered. The generalized modal coordinate  $q$  associated with the mode shape  $\Phi$  of interest for the forced response is assumed to have the following complex harmonic form:

$$q = q^* e^{j\omega t}, \text{ with } q^* \text{ complex.} \quad (19)$$

Seeking a harmonic response in terms of generalized forces (linear aerodynamic behavior assumption), the generalized aerodynamic forces can be approximated as:

$$GAF(t) = \Phi^T F_A(t) \approx F^* e^{j\omega t}, \text{ with } F^* \text{ complex.} \quad (20)$$

In the frequency domain, the structural dynamic equation (3) projected onto the modal basis is now written as:

$$(-\omega^2 \mu + j\omega\beta + \gamma) q^* = F^* \quad (21)$$

and the corresponding frequency response function

$$H = \frac{q^*}{F^*} = \frac{1}{\gamma - \omega^2 \mu + j\omega\beta} \quad (22)$$

gives access to the amplitude of the harmonic motion response due to the combined aerodynamic force, and to the phase angle between force and motion. This equation can be extended to the periodic, multi-harmonic problem and gives, in this case, access to the fundamental and harmonic components of the motion.

A non-linear iterative procedure is needed to simultaneously converge motion and aerodynamic force components. This can be a fixed-point procedure, with or without smoothing, or a Newton procedure, which needs to evaluate the Jacobian matrix of a residual term. In any case, proper convergence of the aerodynamic forces due to vibration is mandatory, in order to correctly evaluate the aerodynamic damping of the involved vibration mode, which is of prominent importance for an accurate prediction of the forced response amplitude.

### Applications

This section presents an overview of several application activities implementing the previously detailed aeroelastic capabilities of *e/sA*. Two applications concern the CFD-CSM coupling procedure presented in Section 0 which has been used within the framework of the ENOVAL and ADEC European projects. Two other items are presented concerning the use of the phase-lagged and multiple frequency phase-lagged sector reduction capabilities detailed previously for stage and multi-stage configurations, during the COBRA Europe-Russia collaboration and within the framework of the *e/sA*-ASO development program with SAFRAN. Finally, some results relative to the forced-response twin methodology are presented. Caution: Due to the confidential features of the presented industrial applications, figures have been suppressed from specific plots.

#### ENOVAL UHBR Fan Flexible Operating Map Prediction

An application of the developed simulation tools based on the coupling of *e/sA/Ael* and MSC/Nastran has been performed for the purpose of computing the hot-shape of a UHBR fan blade within the framework of the European project ENOVAL.

The implemented fan model is shown in Figure 7. On the left side, a view of the aerodynamic sector domain is displayed. The middle plot presents the selected reduced structural model nodes defining the

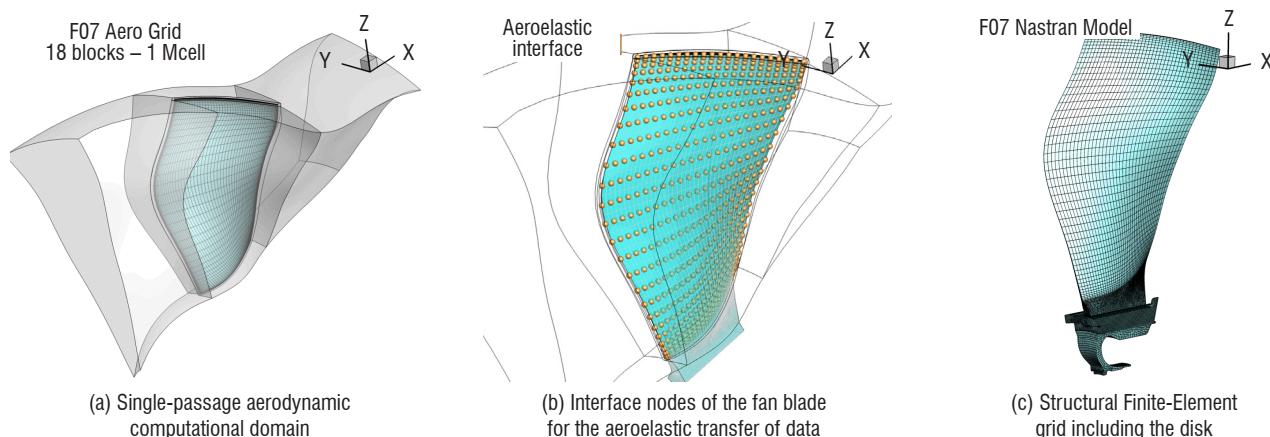


Figure 7 – ENOVAL fan aeroelastic model

aeroelastic transfer model. On the right, the full Finite-Element model used for static non-linear large displacement structural simulations with Nastran is plotted.

The present fully non-linear coupling algorithm has been put to the test for the computation of the massflow to pressure ratio characteristic map of the fan for 100% of the nominal speed line. Contrary to the standard procedure, where a single shape (computed on the nominal operating line) is used for the evaluation of the performance of the fan, the coupled fluid-structure equilibrium is evaluated at each point of the characteristic line, which means that a specific shape is computed at each point of the map, due to modification of the pressure loads.

The *e/sA* solver is implemented using the Smith  $k-\ell$  turbulence model, on an aerodynamic grid including the Outlet Guide Vane (OGV),

of 1.6 Mio cells. The fan performance for ground conditions computed with flexible shapes is compared in Figure 8 to those obtained with a single rigid shape for all operating points of the speed line.

Reynolds effects are taken into account in comparing aerodynamic loads classically obtained with flight conditions and extrapolated to ground conditions in the rigid blade case (Figure 9 in orange and black) and that obtained with the present coupling method, in the flexible blade case, with flight conditions (in blue).

The impact of taking into account flexibility is visible in Figure 8 (orange line: rigid computation, blue line: flexible computation). Differences in terms of maximum pressure ratio and blocking massflow occur, which are related to the variation in blade shape due to flexibility. In particular, blade twist evolves with the pressure ratio in the case of a flexible computation, whereas it remains fixed at its design value in the rigid computation. In the flexible case, an increase in the twist angle under blocking conditions induces a channel section reduction responsible for massflow reduction with respect to the rigid simulation. For high-loaded conditions, flexibility induces a tip gap reduction, leading to better blade efficiency and a higher maximum pressure ratio.

However, one bottleneck for the generalization of the procedure for the entire fan map is the robustness of the mesh deformation process, due to the large variations in the fan shape, especially considering the fan tip gap region, which may vary considerably, inducing large mesh stretching (Figure 9). One clue for the extension of the procedure will be the improvement of mesh deformation technique robustness and efficiency.

### CleanSky II / ADEC CROR Non-Linear Hot Shape Prediction

The present CFD-CSM coupling procedure has also been implemented within the framework of the CleanSky 2 ADEC European project, for the purpose of predicting fan blade hot shapes of the AIPX7 Airbus CROR model shown in Figure 10, tested at the Z49 rig in the S2Ma ONERA wind-tunnel facility [32][59].

For this study, non-linear structural modelling has been implemented in coupling *e/sA* using the solution SOL400 of MSC/NASTRAN, in order to take into account geometric non-linear large displacement

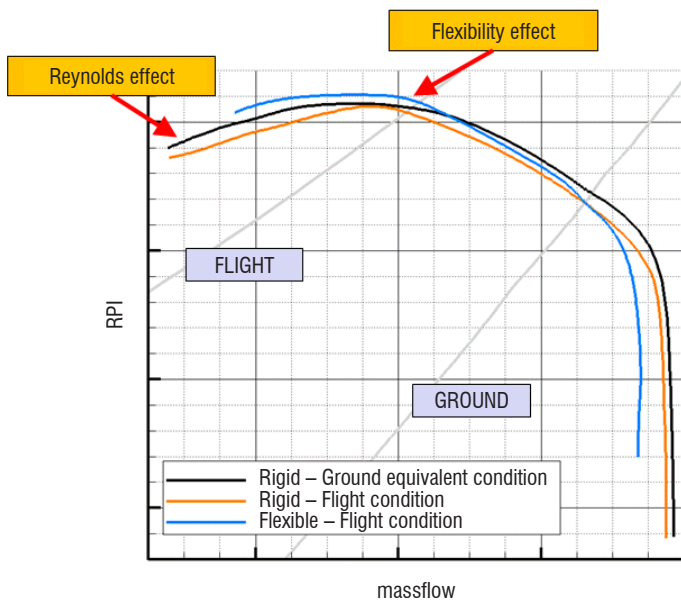


Figure 8 – Influence of the aeroelastic flexibility effect on the characteristic line at 100% Nn

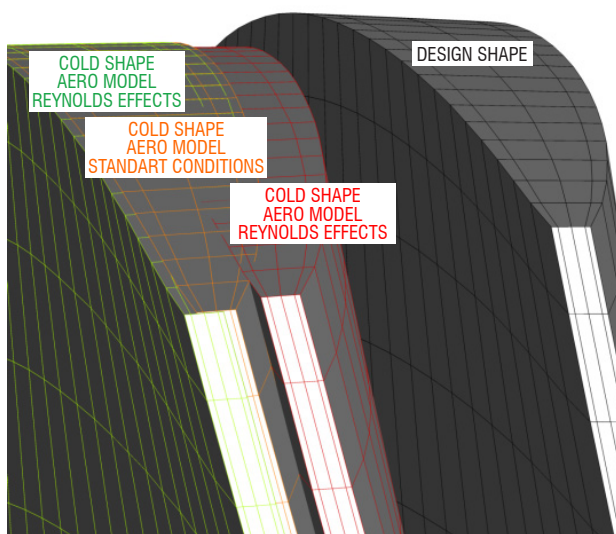


Figure 9 – Blade tip deformations with respect to the rigid design shape.

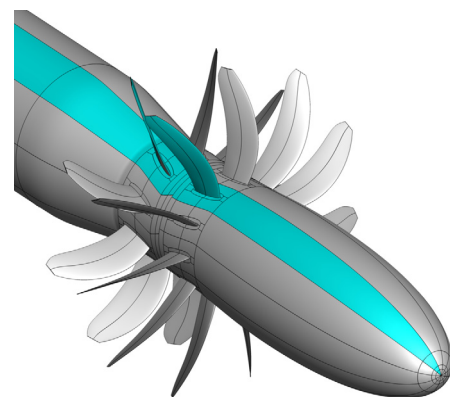


Figure 10 – Full AIPX7 CROR model and single sector model highlighted in cyan

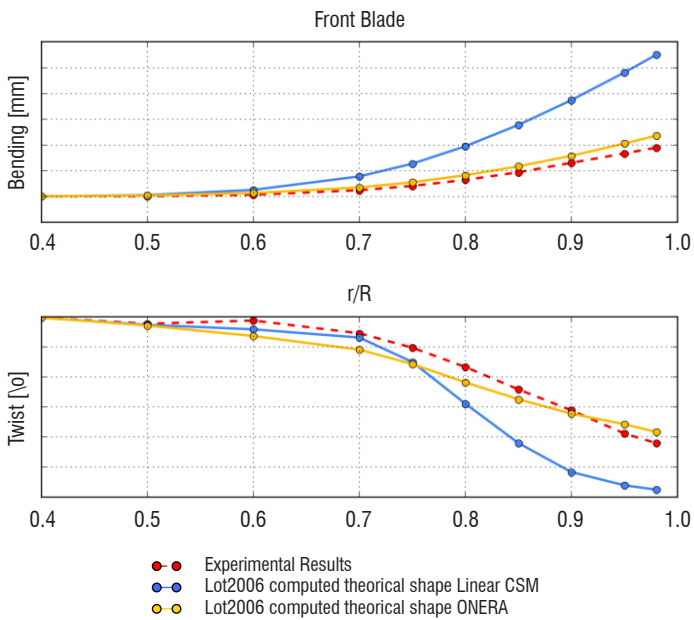
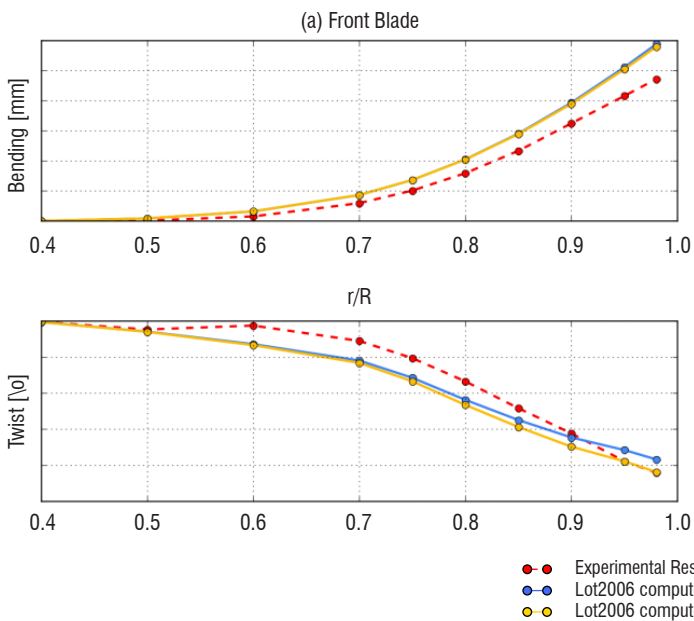


Figure 11 – Comparison between CFD-CSM coupling simulation and experimental results for the AIXP7 front blade at Z49 rig @ cruise conditions  $Ma = 0.75$

effects. In order to highlight the need for non-linear structural modeling in hot shape predictions in this case, Figure 11 shows a comparison between the blade displacements, in terms of bending (top) and twist angle (bottom), obtained using linear CSM (in blue) and nonlinear CSM (in orange) during hot shape computations for the front rotor blade, in comparison with the experimental data in dashed red lines. The selected operating point for this comparison is located at  $Ma = 0.75$ , for a rotation speed of 4510 rpm, at  $0^\circ$  angle of attack. The linear approach overestimates both the blade bending and blade twist by a factor 2. In comparison, non-linear results fit the experimental data very well.

During this study, manufactured blade shape measurements were performed by Airbus using the Z49 test facility. Part of the work



was dedicated to evaluating the consequences of manufacturing uncertainties on numerical hot shape prediction. Figure 12 (a) shows blade deformation comparison, in terms of bending (top) and twist (bottom) versus blade span for the front rotor blade.

The blue and orange curves respectively depict the computed deflection using the CAD shape and the experimental shape. Although fair agreement with the experimental data is observed for both models, taking into account the real manufactured shapes improves the results for twist angle in the blade tip region. Results for the rear blade are shown in Figure 12 (b). Experimental and numerical results are in good agreement with regard to the bending, but major discrepancies are observed with regard to the twist. It seems that a physical phenomenon is missed by the numerical simulations. First investigations tend to show that the blade vortex interaction may have an impact on the blade displacements, but the mixing plane boundary conditions prescribed at the front and rear rotor interface, which forces a steady solution in the CFD computations, does not allow this unsteady interaction to be taken into account.

Work is now ongoing in order to take into account this phenomenon using  $360^\circ$  simulations, and to perform numerical restitutions of unsteady blade deformations for experimental operating points with nonzero angle of attack.

### COBRA Contrafan Aeroelastic Stability Analysis

ONERA is a partner in the COBRA Europe-Russia cooperative research project, in collaboration with SAFRAN, DLR, CIAM and COMOTI. The purpose of COBRA is to design a high by-pass ratio (15-25) contra-fan resulting in much lower blade tip speed and blade count, able to improve aerodynamic and acoustic efficiency. This section presents the activity carried out as part of the work package WP4 of COBRA to assess the aeroelastic stability of Version V4bis of the VITAL contrafan designed during the project. Figure 13 presents the geometries of the structure and aerodynamic models. Both front and aft fans are fully metallic and made of titanium.

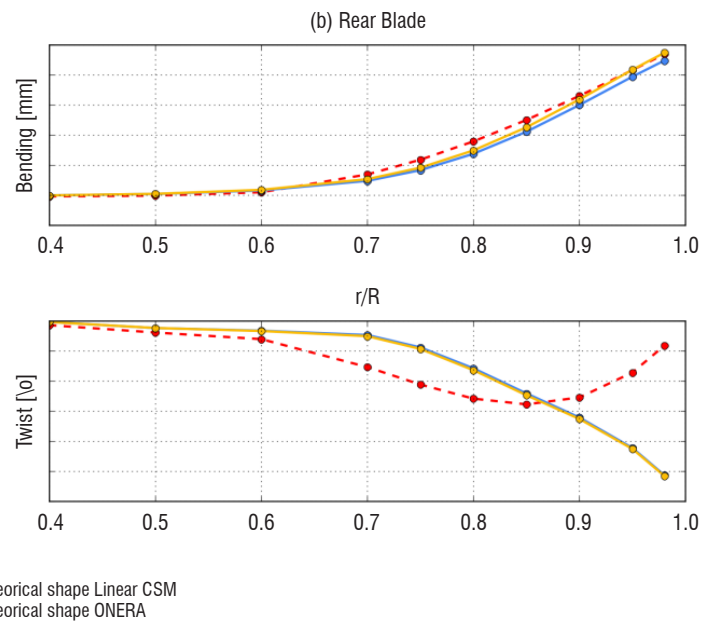
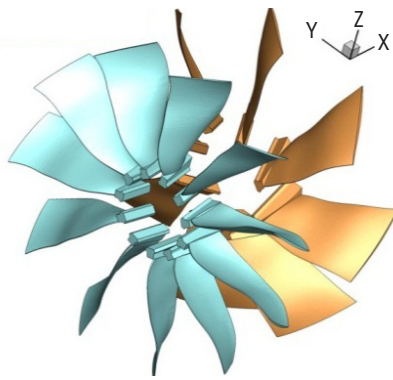
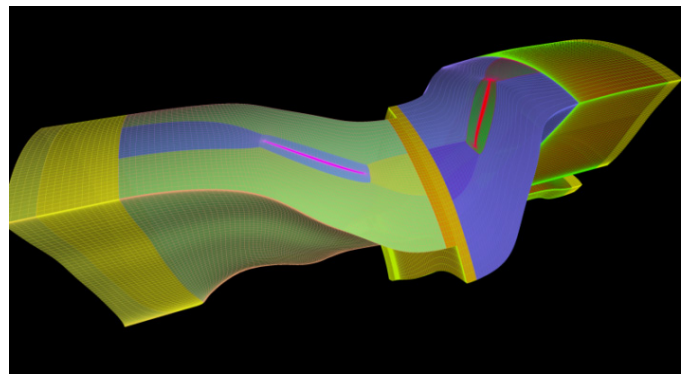


Figure 12 – AIXP7 at Z49 rig – CFD-CSM coupling simulation @ cruise conditions  $Ma = 0.75$ . Comparison between manufactured shape and CAD shape blade deflections

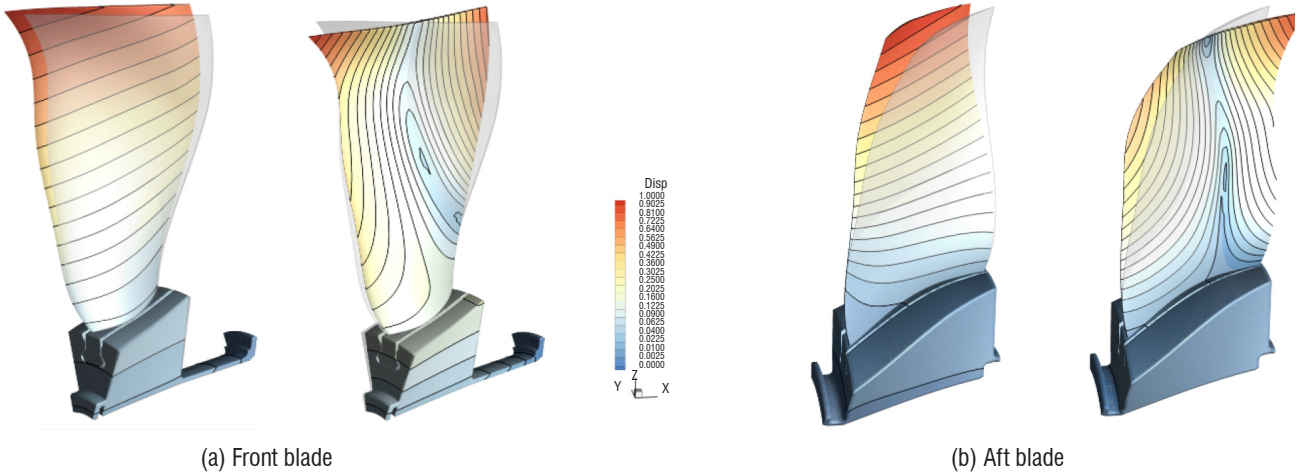


(a) Structural model of front and rear fan



(b) Single-passage aerodynamic computational domain

Figure 13 – COBRA contrafan structural and aerodynamic models



(a) Front blade

(b) Aft blade

Figure 14 – 1F, 1T structural modes @ design point for the nodal diameter 0

For aeroelastic simulations, finite-element grids have been generated for both blades using an in-house software, and connected to blade disk models provided by COMOTI. NASTRAN SOL106 non-linear static analysis, followed by a normal mode analysis, is performed to obtain the eigenmode basis relative to the non-linear deformed shape, including large displacement effects. Figure 14 illustrates the obtained mode shapes at nodal diameter 0, at the aerodynamic design point, for the front blade model (a) and for the aft one (b).

Aerodynamic steady computations have been performed using *e/sA* and compared to equivalent results obtained by the DLR. Some discrepancies have been observed in terms of max massflow values, as

well as max pressure ratio near stall, which may be due to different design evolutions between both models (Figure 15).

Numerical simulations were then performed using *e/sA*, in order to study the aeroelastic stability of the contrafan. In this case, sector reduction was implemented, with classical phase-lagged boundary conditions, assuming no unsteady aerodynamic interactions between both fans. Therefore, an azimuthal average mixing plane boundary condition based on characteristic relations was applied at the row interface, and a single aeroelastic rotating wave was taken into account in each row domain. No provision was made here for rotor-stator unsteady interactions, which was addressed using the multi-chorochronic approach previously detailed.

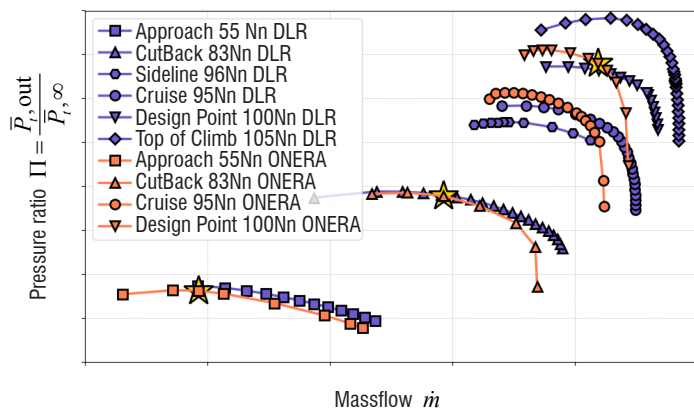


Figure 15 – COBRA contrafan operating map for a different rotation speed

Aeroelastic simulations have been conducted for 3 operating points indicated by the yellow stars in Figure 15. The Dual Time Stepping scheme has been used for the time-consistent resolution of the aerodynamic response to a harmonic forced motion following modal vibrations of each blade row. 26 vibration periods have been computed, in order to reach a conveniently converged periodic solution. First and second bending and first torsion modes have been investigated for each blade row, along with inter-blade dephasing patterns matching 7 (resp., 6) values of nodal diameter over the 11 (resp., 8) possible values for the front (resp., aft) blade. A set of 117 non-linear deformable unsteady aeroelastic URANS simulations requiring the use of phase-lagged boundary conditions have thus been run on 32 cores, each of them corresponding to a typical wall clock computation time of 13 hours.

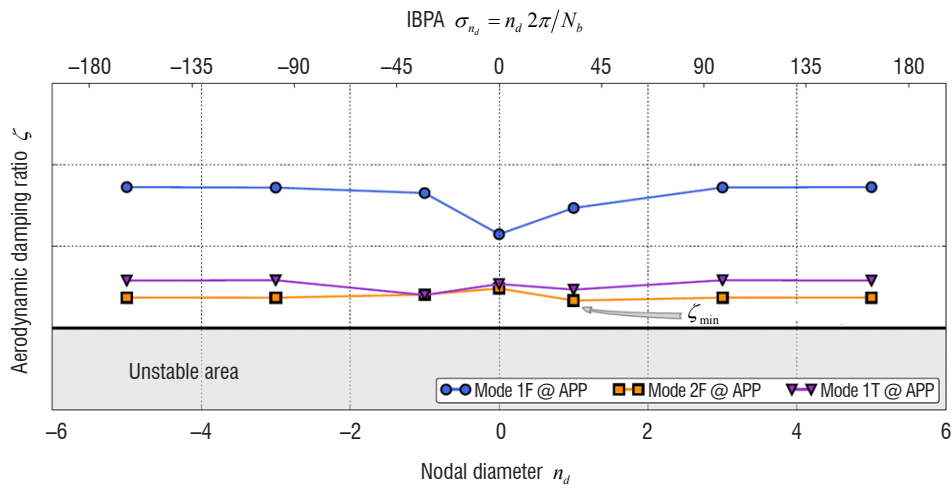


Figure 16 – Approach case – Row 1: aerodynamic damping evolution vs. nodal diameter for 1F, 2F and 1T modes

The harmonic analysis of the generalized aerodynamic forces leads to the extraction of the corresponding damping values, which are plotted in Figure 16, for the Approach operating point, and for the three selected mode shapes (namely the first and second bending and first torsion). The minimal value of aerodynamic damping is obtained in this case for the second bending at nodal diameter 1. However, the full configuration stays clear of flutter in any case investigated here.

### ASTECC2 Multi-Stage Compressor Analysis with Multiple Frequency Phase-Lagged Boundary Conditions

Multiple-frequency phase-lagged boundary conditions have been put to the test (Placzek & Castillon, Aeroelastic Response of a Contrafan Stage Using Full Annulus and Single Passage Models, 2014) (Placzek, Aeroelastic damping predictions for multistage turbomachinery applications, 2014) in the case of the multi-stage axial compressor configuration provided by SAFRAN HE, composed of 6 rows, including a structural strut row R1, an inlet guide vane (IGV) R2 and two rotor/stator stages R3/R4 and R5/R6. Due to the high number of blades of the full 360° configuration (131 blades), a single passage modelling approach is considered for aeroelastic unsteady configurations, in order to keep within acceptable CPU time resources. Aerodynamic interactions between adjacent rows are taken into account with the implementation of the multiple-frequency phase-lagged boundary condition detailed previously.

Several models have been considered to validate the proper use of interface boundary conditions between Rows 1 and 2 and the multiple-frequency phase-lagged boundary condition setup. A full 360° annulus slice model (blue geometry in Figure 17, with 6.5 Mio cells) and the corresponding single passage reduction model (0.54 Mio cells) were first built, in order to cross-validate at a lower cost the implementation of the multiple-frequency phase-lagged boundary conditions. For the 3D configuration (grey geometry in Figure 17), only a single-passage model was used, including 164 blocks and roughly 16 Mio cells.

The steady operating map for the 3D model is presented in Figure 18, with the pressure fields for 3 different operating points. A reference unsteady simulation is then performed with the full 360° annulus slice multi-stage configuration, using 64 processors. The simulation is run for 14.4 revolutions, so that a periodic state can be reached for a total wall-clock time of about 10 days. This simulation is compared to the equivalent single passage simulation performed using multiple frequency phase-lagged boundary conditions to allow for the propagation of blade passage perturbation rotating waves. In this case, a maximum of two spinning modes is considered, corresponding to the rotating waves produced by the blade-passing of the two adjacent rows with nonzero relative speed. For all spinning modes, 48 harmonics are computed with a low value of the relaxation coefficient to

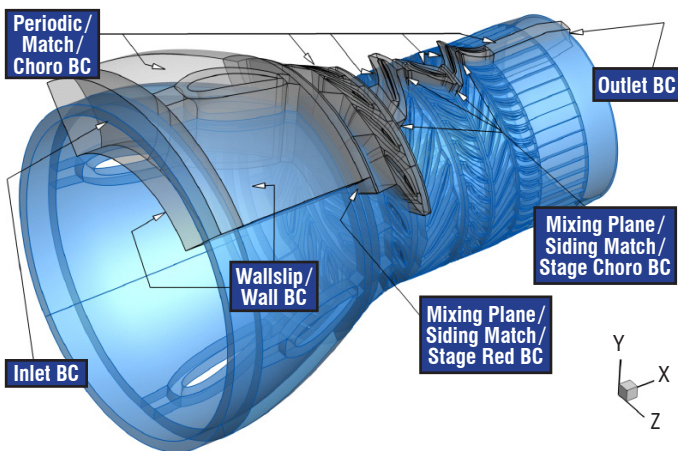


Figure 17 – SAFRAN HE multistage compressor configuration: single passage reduction (grey) vs. 360° full annulus slice model (blue)

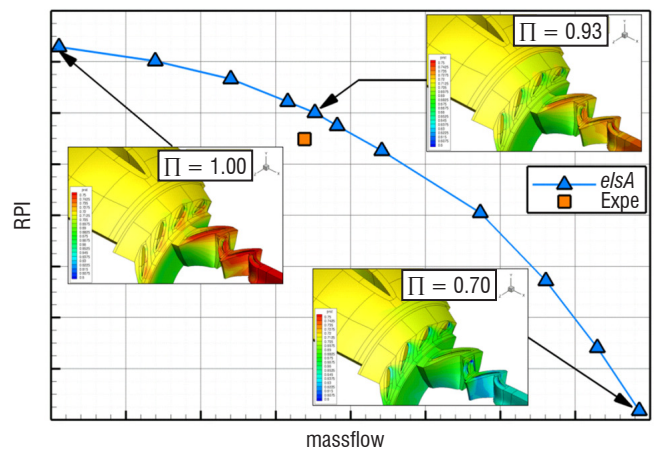


Figure 18 – Compressor operating map of the 3D single-passage model

ensure proper convergence. Due to the small value of the relaxation coefficient, the transient is longer than for the full annulus simulation, but a periodic state is reached before the end of the 14.4 revolutions. The computation is run on only 14 processors, for a global wall-clock time of 2 days and 8 hours.

Figure 19 presents, at the pressure time, histories recorded on numerical pressure sensors located at the mid chord of each blade (#04 on R1, #10 on R2, #18 on R3, #26 on R4, #34 on R5 and #42 on R6). The results from the full 360° annulus slice model are compared as a reference to the single-passage reduction solution using the multiple-frequency phase-lagged boundary conditions involving two different values of the relaxation parameter  $\alpha$ .

The agreement between both solutions is satisfactory in terms of global frequency content and, to a lesser extent, in terms of amplitude, see Figure 20. The blue curve corresponds to the multiple frequency phase-lagged case, with the highest value of relaxation coefficient  $\alpha = 0.5$ , which however leads to a divergence of the simulation. The spectral analyses of the time histories at the bottom reveal that, apart from an unexpected asynchronous frequency observed at 7.5 Engine Order ( $EO = f / \Omega$ ) with the 360° simulation in the first 4 rows, the spectral content is driven by the blade pas-

sage frequencies in the different blade rows, with the main contribution of the 16<sup>th</sup> EO and its first harmonic (32<sup>nd</sup> EO) in R1 and R2, because of the blade-passage effect of the first rotor R3 made up of 16 blades. In blade row R3 the 16<sup>th</sup> EO due to the passage of R2>R3 and the 29<sup>th</sup> EO due to the passage of R4>R3 are dominant, with the additional 45<sup>th</sup> EO induced by the combination of the 16<sup>th</sup> and 29<sup>th</sup> EO. The blade passages of R3>R4 and R5>R4 induce significant levels of pressure fluctuations at the 16<sup>th</sup> and 23<sup>rd</sup> EO, respectively, in blade row R4 and, finally, in blade row R5, the 29<sup>th</sup> and 43<sup>rd</sup> EO induced by the blade passage of R4>R5 and R6>R5 contribute mainly, whereas only the 23<sup>rd</sup> EO due to the passage of R5>R6 is visible in blade row R6.

It must be pointed out that a small relaxation factor ( $\alpha = 0.1$ ) is necessary to ensure the robustness of the multiple-frequency phase-lagged approximation for long-time simulations and to avoid the apparition of spurious frequencies. Moreover, the full 360° annulus model response exhibits an asynchronous frequency generated by a separated flow area downstream from R2 that cannot be captured by the multiple-frequency phase-lagged approximation.

The unsteady rigid simulation has also been performed in the case of the 3D single passage model for the intermediate operating point

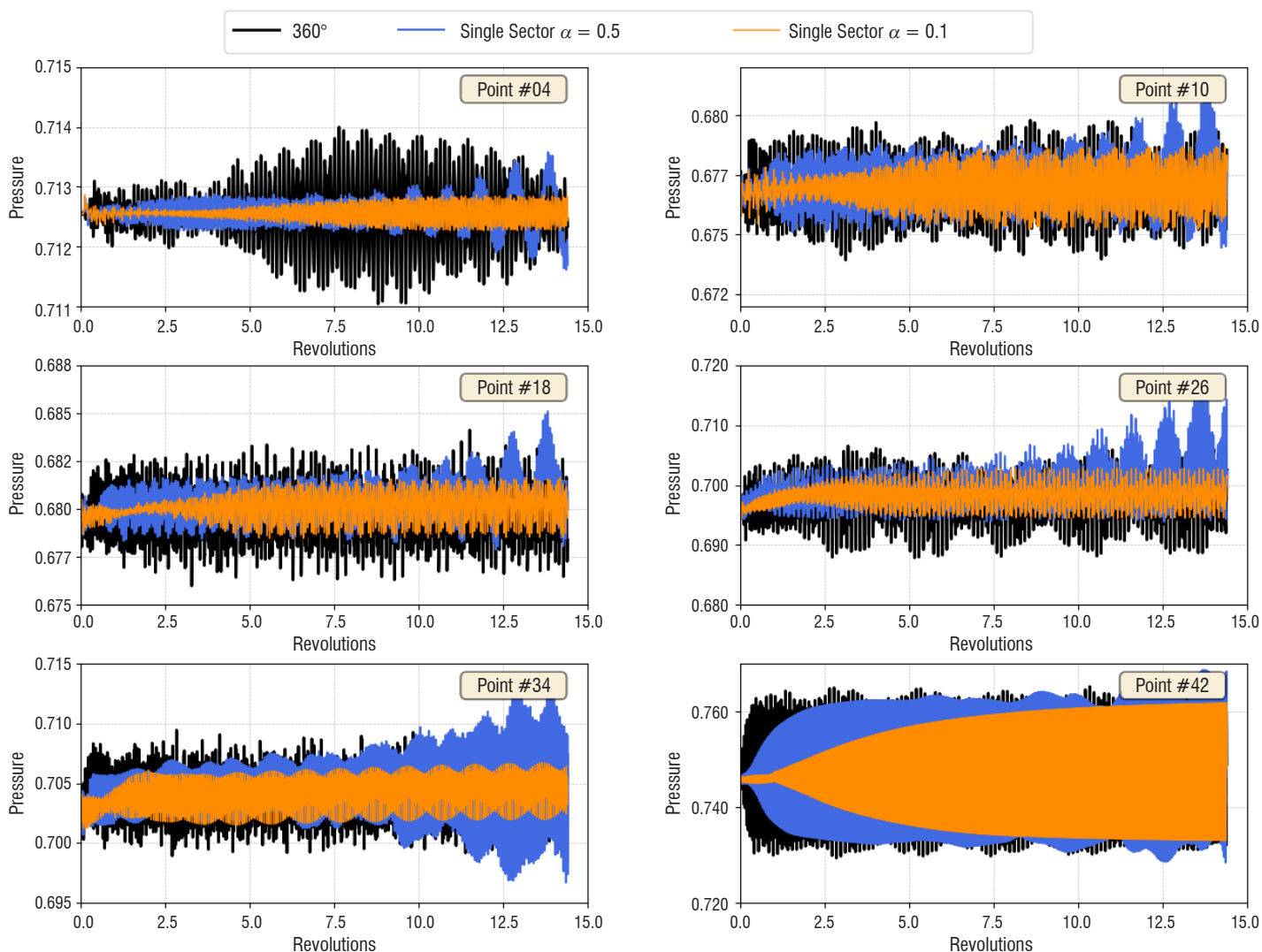


Figure 19 – Pressure-time histories of blade skin sensors for the full 360° annulus slice model vs. the single-passage slice model with different values of the relaxation parameter

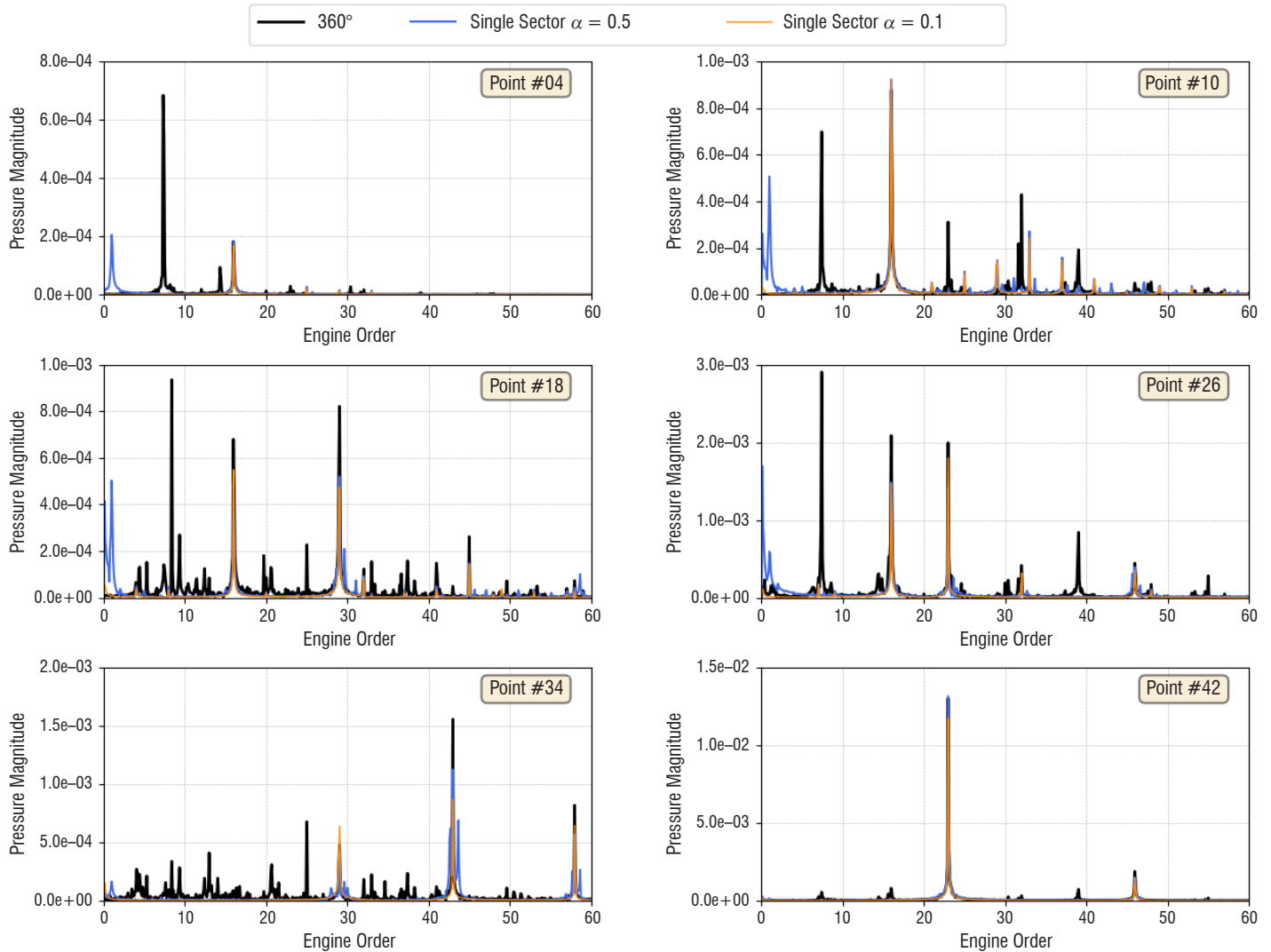


Figure 20 – Frequency content of the pressure blade skin sensors for the full 360° annulus slice model vs. the single-passage slice model with different values of the relaxation parameter

on the speedline shown in Figure 18. Figure 21 and Figure 22 present, respectively, the time histories and spectral analyses recorded by the same pressure sensors as those monitored with the 360° slice model. These simulations, however, have not been validated against the full 360° 3D configuration equivalent results, for clear CPU cost reasons. The simulation for the single-passage model run with 90 processors indeed requires a total wallclock time of 20 days to cover 30 revolutions.

The use of the multiple-frequency phased-lagged boundary condition approach for a multi-stage compressor configuration has been validated on a slice reduction of the machine against full 360° annulus model results. This validation, however, has been made for the rigid case, due to the lack of data for a proper aeroelastic validation setup. Moreover, a demonstration of the capability of the multiple frequency phase-lagged approach has also been made on the 3D single-passage model.

A fully-aeroelastic validation implementing a modal vibration of a row, although already conducted on the simpler VITAL contrafan stage configuration [53], has still to be conducted on the ASTEC2 case,

in order to fully validate the approach for aero-structure problems of multi-stage configurations.

### Forced-Response Problems

The twin method presented in the previous section has been tested in the case of a transonic gust-generator experimental system [37], developed within the framework of the SFWA European project, implementing a basic forced-response problem.

Figure 23 presents the experimental device that consists of an aero-elastic model (foreground), comprising an OAT15A airfoil placed on a mechanical suspension system, and a gust generator (background), comprising a set of two NACA airfoils oscillating in phase. The arrow shows the propagation of the gust. The system is located in the ONERA S3Ch transonic wind-tunnel. The two front airfoils of the Gust Generator device synchronously oscillate in pitch to generate a gust flow that excites the aft profile. This airfoil is free to move according to its mechanical suspension system properties, allowing a pitch and heave motion. The aerodynamic excitation due to the wake thus leads to a periodical forced response motion of the OAT airfoil.

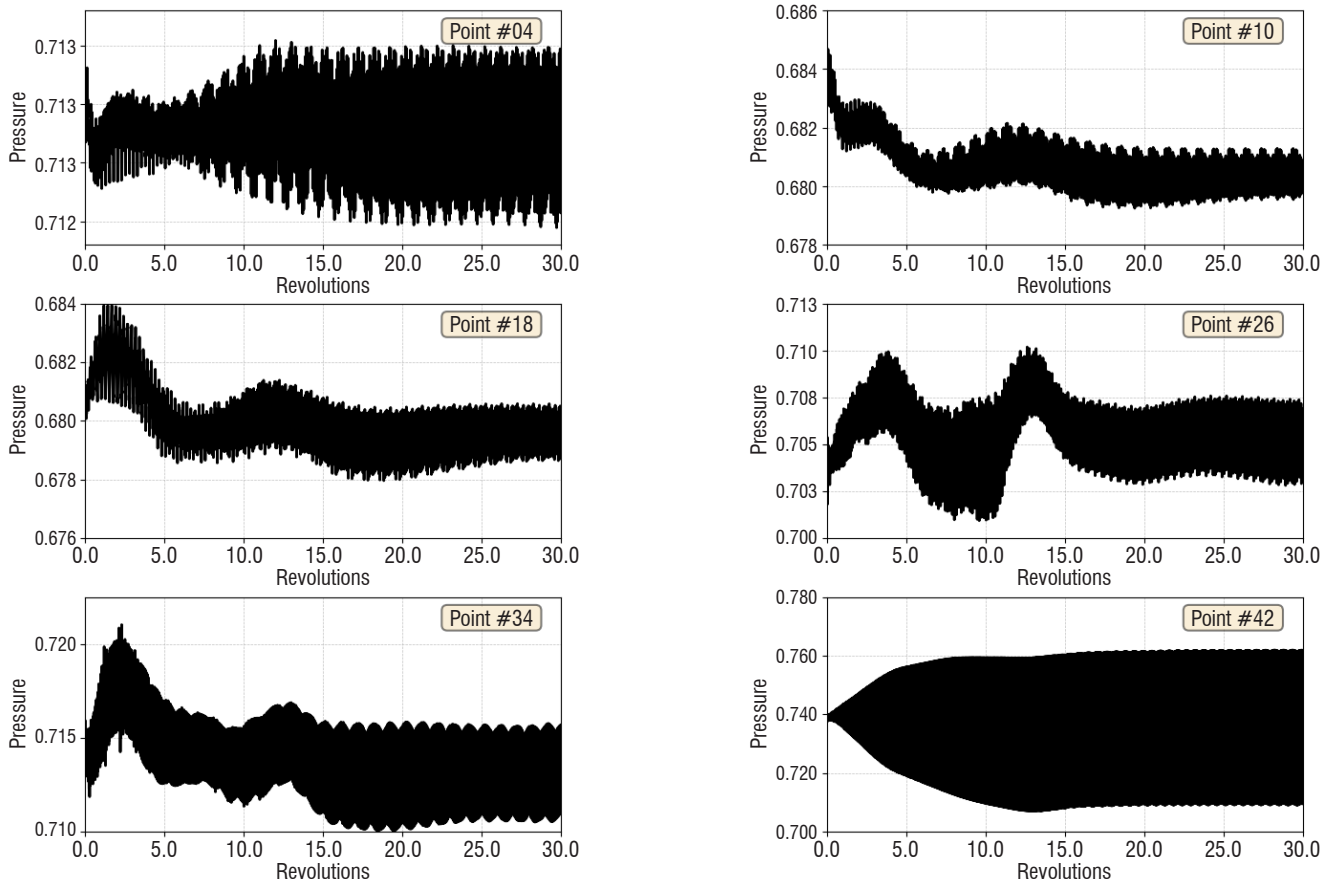


Figure 21 – Pressure time histories of blade skins sensors for the 3D single passage model with  $\alpha = 0.1$

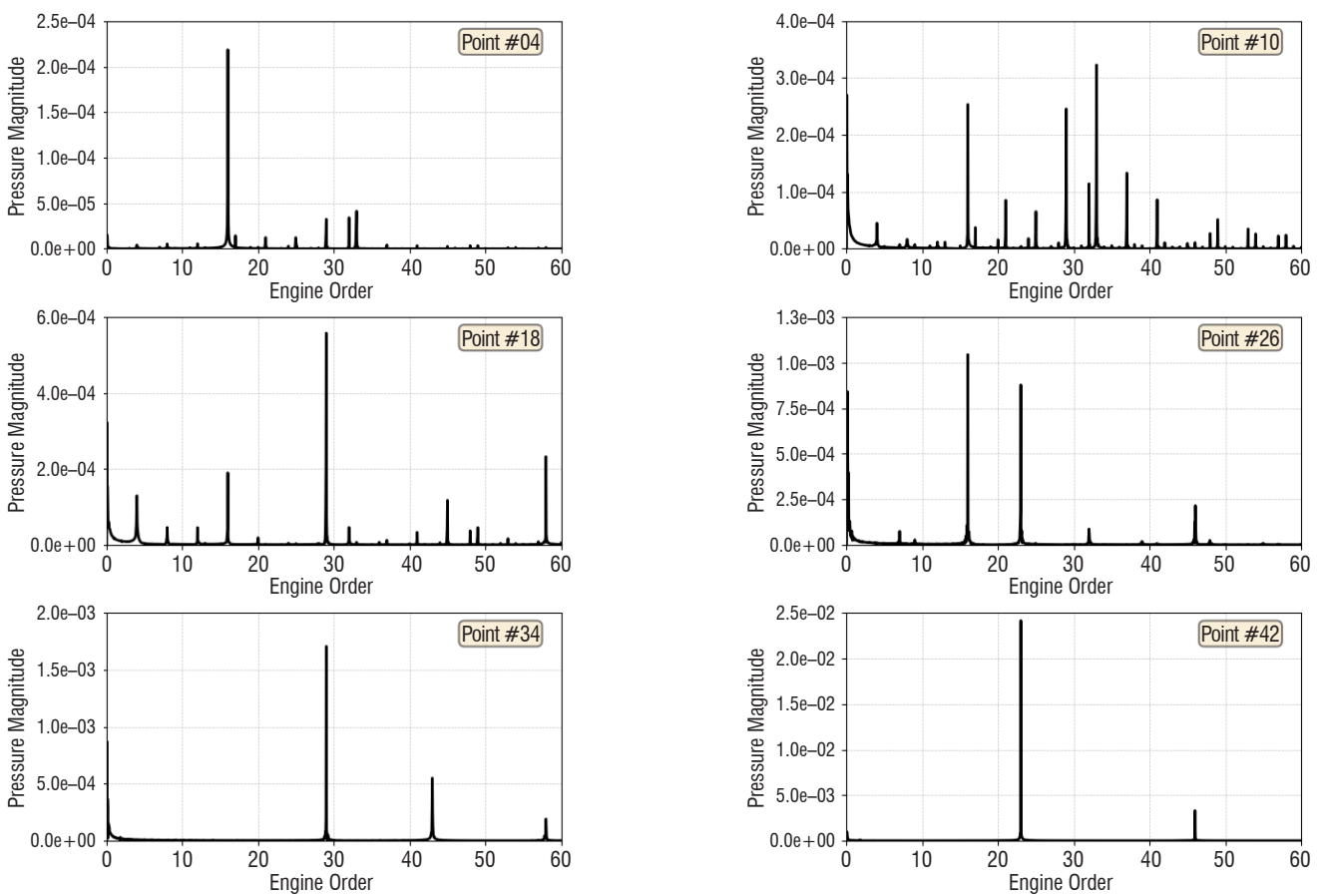


Figure 22 – Frequency content of the pressure blade skin sensors for the 3D single-passage model with  $\alpha = 0.1$

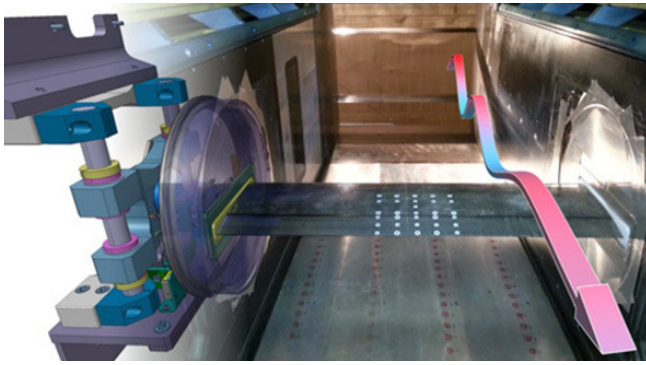


Figure 23 – SFWA Gust-generator experimental setup

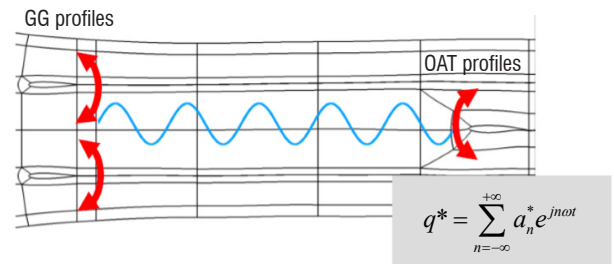


Figure 24 – Twin forced-response procedure implementing gust excitation and prescribed forced motion of the excited profile

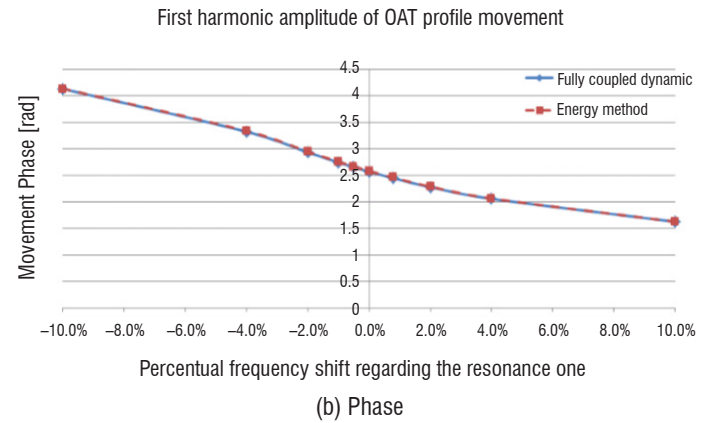
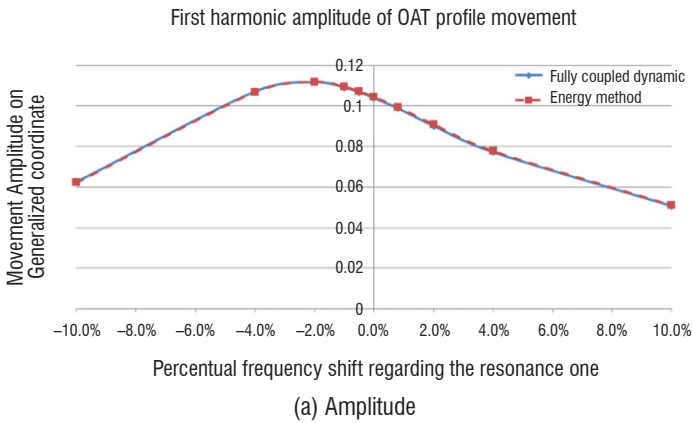


Figure 25 – Forced response close to the coincidence frequency

The effect of gust fields on the aerodynamic and aeroelastic behavior of the model was analyzed and the experimental data was delivered to ONERA's main partners (Airbus and Dassault Aviation) for the validation of their numerical methods.

A twin simulation is conducted on this configuration, including a harmonic forced motion of the gust generator airfoil doublet, as well as a periodic forced motion of the OAT profile, whose harmonic content is periodically updated to balance the dynamic system forced-response equations (Figure 24). The gust generator is excited at frequency 25 Hz and amplitude 3°, for a Mach number of 0.7294. The values of the generalized mass, damping and stiffness for the excited heave mode are:  $\mu = 0.01$ ,  $\beta = 0.115$ ,  $\gamma = 242.94$ .

Figure 25 presents the results of the twin simulation (in red) compared to those obtained with the fully-coupled direct method in time domain (in blue). Amplitude levels (a) and phase (b) of the first harmonic component of motion are given, for various excitation frequencies, close to the heave modal frequency (–10% to +10% range). The maximum amplitude is obtained, as expected, near the modal frequency, but a slight deviation is observed due to the impact of the aerodynamic stiffness, which induces a small offset. The agreement with the fully coupled method is excellent.

It must be noticed, however, that the convergence of the method is made all the more difficult if the structural damping is small, which leads to high levels of forced response. This point must be improved for a robust use of the method in the case of turbomachinery forced-response problems, such as rotor stator interaction, inlet distortion or crosswind-induced response.

## Perspectives

Several activities are currently being carried out in the Aeroelasticity Modelling and Simulation research unit of ONERA to address new topics concerning the aeroelastic behavior of turbomachines. One main issue concerns the prediction of the aeroelastic stability and of the forced response of turbomachines, especially fans, facing distorted inlet conditions. In particular, due to inhomogeneous total pressure and velocity at the inlet, large levels of structural forced response may be observed, which must be studied for safety reasons. These conditions may occur, in various circumstances, such as crosswind conditions, impinging wakes, boundary layer ingestion (BLI), or even interactions with ground-induced vortices (Figure 26). In these cases, the basic assumption of cyclic symmetry retained for sector reduction modelling is questionable, and 360° modelling may be mandatory.

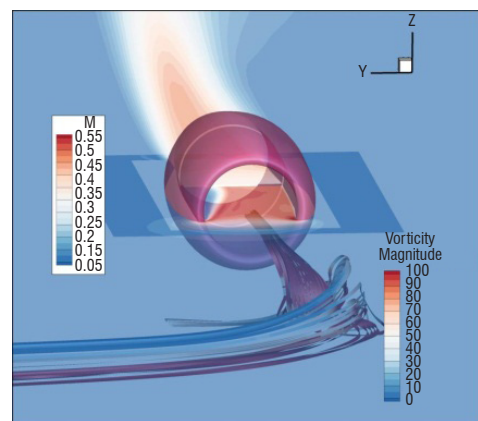


Figure 26 – Current activities on fan-vortex interaction [38]

On the other hand, new activities are currently being conducted, in order to build a modular aeroelastic simulation environment, whose objective is to deliver new simulation capabilities in coupling several individual modules for the resolution of aeroelastic problems. This work is intended to provide a tool versatile enough to extend the coupling solution currently available with *e/sA* to other non-linear aerodynamic solvers (newly developed CFD2030 aerodynamic codes) and non-linear structural solvers. Such a tool will potentially provide access to an aerodynamic modeling alternative to URANS, such as LES, or Lattice-Boltzmann, and to innovative techniques such as the Immersed Boundary Method for aeroelasticity. Moreover, this modular architecture will allow new innovative algorithms for fluid-structure transfers and mesh deformation strategy to be implemented more easily, without costly additional *e/sA* C++ Kernel development. This architecture will rely on a CGNS compliant data model, specifically extended to fluid-structure coupling, and modular extensions using Python interfaces (Figure 27).

## Conclusion

The aim of this paper was to present the current development status and research activities concerning the modelling of aeroelastic phenomena of rotating machines recently conducted at ONERA. In the second part, we have presented some basic capabilities of the *e/sA* ONERA aerodynamic solver, and then those of the specific aeroelastic extension of *e/sA*, Ael.

Next, we have first described specific capabilities recently implemented for the non-linear coupling of the *e/sA* non-linear aerodynamic solver and MSC/Nastran, allowing for the resolution of non-linear large-displacement static problems. Then, dynamic functionalities for unsteady weak coupling aeroelastic simulations, in the case of stage and multi-stage turbomachine configurations and for forced

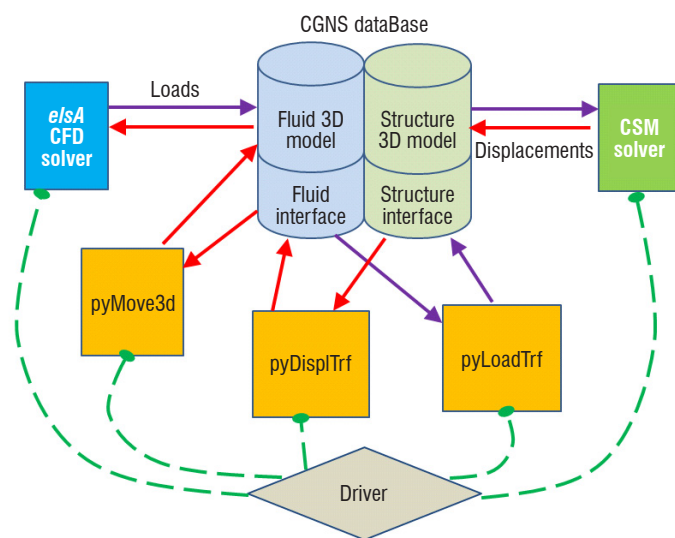


Figure 27 – Targeted fluid-structure modular architecture for the communications between fluid and structural solvers

response problems, have been presented. These functionalities have been implemented in several European and national projects, such as COBRA, ENOVAL, CS2-ADEC and *e/sA*/ASO.

One perspective for future work within the framework of turbomachine aeroelastic problems concerns the taking into account of the impact of distorted inflow on the aeroelasticity of fans and openrotors, especially with regard to forced response. This topic will be addressed within the framework of the ENOVAL European project in particular. Secondly, the extension of aeroelastic coupling capabilities to fully non-linear fluid-structure modelling is currently under construction and will provide larger modelling capabilities for aeroelastic problems ■

## Acknowledgements

The studies presented in this article have been partially funded by Airbus, Safran and ONERA, which are co-owners of the software.

## Nomenclature

$\theta$	(azimuth angle)
$N$	(number of sectors of the row)
$\Phi$	(deformation mode shapes)
$M, D, K$	(structural mass, damping, stiffness matrices)
$q$	(generalized coordinates)
$F_a(t)$	(aerodynamic force)
$\alpha$	(relaxation coefficient)
$u$	(structural displacements)
$w$	(aerodynamic field)
$\sigma_n$	(inter-blade phase angle)
$X = \begin{bmatrix} u \\ w \end{bmatrix}$	(fluid-structure variables)

## References

- [1] A. GROLET, F. THOUVEREZ - *On a New Harmonic Selection Technique for Harmonic Balance Method*. Mechanical Systems and Signal Processing, Vol. 30, pp. 43-60, 2012.
- [2] M. A. BAKHLE, T. S. REDDY, R. CORONEOS, J. B. MIN, A. J. PROVENZA, K. P. DUFFY, G. S. HEINLEIN - *Aeromechanics Analysis of a Distortion-Tolerant Fan with Boundary Layer Ingestion*. AIAA Aerospace Sciences Meeting, 2018.
- [3] M. A. BAKHLE, T. S. REDDY, M. RULA, M. CORONEOS - *Forced Response Analysis of a Fan with Boundary Layer Inlet Distortion*. 50<sup>th</sup> AIAA/ASME/SAE/ASEE Joint Propulsion Conference, 2014.
- [4] M. A. BAKHLE, R. SRIVASTAVA, T. G. KEITH, G. L. STEFKO, & J. JANUS - *Development of an Aeroelastic Code Based on an Euler/Navier-Stokes Aerodynamic Solver*. NASA Technical Memorandum, NASA, November 1996.
- [5] T. BERTHELON, A. DUGEAI, J. LANGRIDGE, F. THOUVEREZ - *Fan Forced Response due to Inlet Ground Vortex Ingestion*. 53<sup>rd</sup> 3AF International Conference on Applied Aerodynamics. Salon de Provence, France, 2018.
- [6] C. BRÉARD, M. VAHDATI, A. I. SAYMA, M. IMREGUN - *An Integrated Time-Domain Aeroelasticity Model for the Prediction of Fan Forced Response Due to Inlet Distortion*. ASME Turbo Expo 2000: Power for Land, Sea, and Air, 2000.
- [7] L. CAMBIER, S. HEIB, S. PLOT - *The ONERA elsA CFD Software: Input from Research and Feedback from Industry*. Mechanics & Industry, 14(3), 159-174. Retrieved from dx.doi.org/10.1051/meca/2013056, 2013.
- [8] V. CARSTENS - *Computations of Unsteady Transonic 3D-Flow in Oscillating Turbomachinery Bladings by an Euler Algorithm with Deforming Grids*. 7<sup>th</sup> International Symposium on Unsteady Aerodynamics and Aeroelasticity of Turbomachines. Fukuoka, Japan, 25-29 September 1994.
- [9] F. O. CARTA - *Coupled Blade-Disk-Shroud Flutter Instabilities in Turbojet Engine Rotors*. Journal of Engineering for Gas Turbines and Power, 89(3), 419-426. Retrieved from dx.doi.org/10.1115/1.3616708, 1967.
- [10] L. CASTILLON, N. GOURDAIN, X. OTTAVY - *Multiple-Frequency Phase-Lagged Unsteady Simulations of Experimental Axial Compressor*. Journal of Propulsion and Power, 31(1), 444-455. Retrieved from dx.doi.org/10.2514/1.B35247, January 2015.
- [11] W. S. CLARK, K. C. HALL - *A Time-Linearized Navier-Stokes Analysis of Stall Flutter*. ASME Journal of Turbomachinery, 122, 467-476, 2000.
- [12] A. DUGEAI - *Turbomachinery Aeroelastic Developments and Validations using ONERA elsA Solver*. International Forum on Aeroelasticity and Structural Dynamics. Stockholm, Sweden, 18-20 June 2007.
- [13] A. DUGEAI, S. VERLEY - *Numerical Evaluation of CRORs Dynamic Loads Induced by Whirl Flutter*. 3AF CEAS Greener Aviation. Brussels, Belgium, 2014.
- [14] A. DUGEAI, A. MADEC, A. S. SENS - *Numerical Unsteady Aerodynamics for Turbomachinery Aeroelasticity*. 9<sup>th</sup> International Symposium on Unsteady Aerodynamics, Aeroacoustics and Aeroelasticity of Turbomachines. Lyon, 4-7 September 2000.
- [15] A. DUGEAI, Y. MAUFFREY, F. SICOT - *Aeroelastic Capabilities of the elsA Solver for Rotating Machines Applications*. International Forum on Aeroelasticity and Structural Dynamics. Paris, France, June 2011.
- [16] K. EKICI, K. C. HALL - *Nonlinear Analysis of Unsteady Flows in Multistage Turbomachines using Harmonic Balance*. AIAA Journal, 45(5), 1047-1057, 2007.
- [17] J. I. ERDOS, E. ALZNER, W. MCNALLY - *Numerical Solution of Periodic Transonic Flow through a Fan Stage*. AIAA Journal, 15(11), 1559-1568, 1977.
- [18] M. ERRERA, A. DUGEAI, P. GIRODROUX-LAVIGNE, J. GARAUD, M. POINOT, S. CERQUEIRA, G. CHAINERAY - *Multi-Physics Coupling Approaches for Aerospace Numerical Simulations*. AerospaceLab, 2(2), 1-16, 2011.
- [19] G. A. GEROLYMOS - *Filtered Chorochronic Interface as a Capability for 3-D Unsteady Throughflow Analysis of Multistage Turbomachinery*. International Journal of Computational Fluid Dynamics, 27(2), 100-117, 2013.
- [20] G. A. GEROLYMOS, G. J. MICHON, J. NEUBAUER - *Analysis and Application of Chorochronic Periodicity in Turbomachinery Rotor/Stator Interaction Computations*. AIAA Journal, 18(6), 1139-1152, 2002.
- [21] G. GEROLYMOS, I. VALLET - *Validation of 3-D Euler Methods for Vibrating Cascade Aerodynamics*. ASME Turbo Expo, 1994.
- [22] M. B. GILES - *Calculation of Unsteady Wake/Rotor Interaction*. Journal of Propulsion and Power, 4(4), 356-362, 1988.
- [23] P. GIRODROUX-LAVIGNE, A. DUGEAI - *Fluid-Structure Coupling Using Chimera Grids*. International Forum on Aeroelasticity and Structural Dynamics. Seattle, USA, 21-25 June 2009.
- [24] K. C. HALL, E. F. CRAWLEY - *Calculation of Unsteady Flows in Turbomachinery using the Linearized Euler Equations*. AIAA Journal, 27(6), 777-787, 1989.
- [25] K. C. HALL, B. LORENCE - *Calculation of Three-Dimensional Unsteady Flows in Turbomachinery Using the Linearized Harmonic Euler Equations*. Journal of Turbomachinery, 115(4), 800-809, October 1993.
- [26] K. C. HALL, P. D. SILKOWSKI - *The Influence of Neighboring Blade Rows on the Unsteady Aerodynamic Response of Cascades*. Journal of Turbomachinery, 119(1), 85-93, 1997.
- [27] K. C. HALL, J. P. THOMAS, W. S. CLARK - *Computation of Unsteady Nonlinear Flows in Cascades using a Harmonic Balance Technique*. AIAA Journal, 40(5), 879-886, 2002.
- [28] H. J. HASSIG - *An Approximate True Damping Solution of the Flutter Equation by Determinant Iteration*. Journal of Aircraft, 8(11), 885-889, 1971.
- [29] L. HE - *An Euler Solution for Unsteady Flows Around Oscillating Blades*. Journal of Turbomachinery, 112(4), 714-722, 1990.
- [30] L. HE - *Method of Simulating Unsteady Turbomachinery Flows with Multiple Perturbations*. AIAA Journal, 30(11), 2730-2735, 1992.
- [31] L. HE, W. NING - *Efficient Approach for Analysis of Unsteady Viscous Flows in Turbomachines*. AIAA Journal, 36(11), 2005-2012. Retrieved from <https://doi.org/10.2514/2.328>, November 1998.
- [32] G. P. HERRICK - *Assessing Fan Flutter Stability in Presence of Inlet Distortion Using One-way and Two-way Coupled Methods*. 50<sup>th</sup> AIAA/ASME/SAE/ASEE Joint Propulsion Conference, 2014.
- [33] X. Q. HUANG, L. HE, D. L. BELL - *Influence of Upstream Stator on Rotor Flutter Stability in a Low Pressure Steam Turbine Stage*. Journal of Power and Energy, 220(1), 25-35, 2006.
- [34] M. KARPEL - *Design for Active Flutter Suppression and Gust Alleviation Using State-Space Aeroelastic Modeling*. AIAA Journal of Aircraft, 19, 221-227, 1982.

- [35] R. E. KIELB - *Forced Response Design Analysis. Aeroelasticity in Axial-Flow Turbomachines*. Rhode-Saint-Genese, Belgium: von Karman Institute for Fluid Dynamics, 1999.
- [36] K. LEE, M. WILSON, M. VAHDATI - *Numerical Study on Aeroelastic Instability for a Low-Speed Fan*. Journal of Turbomachinery, 139(7), 2017.
- [37] A. LEPAGE, Y. AMOSSE, D. LEBIHAN, C. POUSSOT-VASSAL, V. BRION, E. RANTET - *A Complete Experimental Investigation of Gust Load from Generation to Active Control*. International Forum on Aeroelasticity and Structural Dynamics. Saint Petersburg, Russia, 2015.
- [38] J. G. MARSHALL, M. IMREGUN - *A Review of Aeroelasticity Methods with Emphasis on Turbomachinery Applications*. Journal of Fluids and Structures, 10(3), 237-267, 1996.
- [39] Y. MAUFFREY, A. GEERAERT - *CROR Blade Deformation, part 2: Aeroelastic Computations and Comparison with Experiments*. International Forum on Aeroelasticity and Structural Dynamics. Saint Petersburg, Russia, June 28-July 2 2015.
- [40] M. MESBAH, J.-F. THOMAS, F. THIRIFAY, A. NAERT, S. HIERNAUX - *Investigation of Forced Response Sensitivity of Low Pressure Compressor With Respect to Variation in Tip Clearance Size*. Journal of Turbomachinery, 137(9), 2015.
- [41] S. MOFFAT, W. NING, Y. LI, R. G. WELLS, L. HE - *Blade Forced Response Prediction for Industrial Gas Turbine*. Journal of Propulsion and Power, 21(4), 707-714, July-August 2005.
- [42] R. MORETTI - *Direct Method to Predict the Forced Response in Turbomachinery Compressor*. MSc Thesis, Politecnico di Torino, October 2016.
- [43] A. PLACZEK - *Aeroelastic Damping Predictions for Multistage Turbomachinery Applications*. 29<sup>th</sup> Congress of the International Council of the Aeronautical Sciences. Saint Petersburg. Retrieved from hal-onera.archives-ouvertes.fr/hal-01078504/, 7-12 September 2014.
- [44] A. PLACZEK, L. CASTILLON - *Aeroelastic Response of a Contrafan Stage Using Full Annulus and Single Passage Models*. Journal of Aeroelasticity and Structural Dynamics, 3(2), 1-30. Retrieved from dx.doi.org/10.3293/asdj.2014.30, May 2014.
- [45] A. PLACZEK, A. DUGEAI - *Numerical Prediction of the Aeroelastic Damping using Multi-Modal Dynamically Coupled Simulations on a 360° fan configuration*. International Forum on Aeroelasticity and Structural Dynamics. Paris, 27-30 juin 2011.
- [46] A. I. SAYMA, M. VAHDATI, M. IMREGUN - *An Integrated Nonlinear Approach for Turbomachinery Forced Response Prediction. Part I: Formulation*. Journal of Fluids and Structures, 14(1), 87-101, 2000.
- [47] S. SCHMITT, D. NÜRNBERGER, V. CARSTENS - *Evaluation of the Principle of Aerodynamic Superposition in Forced Response Calculations*. 10<sup>th</sup> International Symposium on Aerodynamics, Aeroacoustics and Aeroelasticity in Turbomachines. Durham (NC), 2003.
- [48] M. SCHUFF, T. LENGYEL-KAMPMANN, N. FORSTHOFER - *Influence of the Steady Deformation on Numerical Flutter Prediction for Highly Loaded and Flexible Fan Blades*. ASME Turbo Expo. Charlotte, North Carolina, USA, 26-30 June 2017.
- [49] F. SICOT, T. GUÉDENEY, G. DUFOUR - *Time-Domain Harmonic Balance Method for Aerodynamic and Aeroelastic Simulations of Turbomachinery Flows*. International Journal of Computational Fluid Dynamics, 27(2), 68-78, 2012.
- [50] S. C. STAPELFELDT, L. DI MARE - *A Method for Modelling Flow Past Non-Axisymmetric Configurations on Reduced Passage Counts*. 13<sup>th</sup> International Symposium on Unsteady Aerodynamics, Aeroacoustics and Aeroelasticity of Turbomachines. Tokyo, 11-14 Septembre 2012.
- [51] S. C. STAPELFELDT, A. PARRY, M. VAHDATI - *Investigation of Flutter Mechanisms of a Contra-Rotating Open Rotor*. Journal of Turbomachinery, 138(5), 2016.
- [52] D.-M. TRAN, C. LIAUZUN, C. LABASTE - *Methods of Fluid-Structure Coupling in Frequency and Time Domains using Linearized Aerodynamics for Turbomachinery*. Journal of Fluids and Structures, 17(8), 1161-1180. Retrieved from dx.doi.org/10.1016/S0889-9746(03)00068-9, 2003.
- [53] J. M. TYLER, T. G. SOFFRIN - *Axial Flow Compressor Noise Studies*. SAE Transactions, 70(620532), 309-332. Retrieved from dx.doi.org/10.4271/620532, 1962.
- [54] M. VAHDATI, A. I. SAYMA, M. IMREGUN - *An Integrated Nonlinear Approach for Turbomachinery Forced Response Prediction. Part II: Case Studies*. Journal of Fluids and Structures, 14(1), 103-125, 2000.
- [55] M. VAHDATI, A. SAYMA, M. IMREGUN, G. SIMPSON - *Multibladerow Forced Response Modeling in Axial-Flow Core Compressors*. Journal of Turbomachinery, 129(2), 412-420, 2005.
- [56] M. VAHDATI, A. SAYMA, J. G. MARSHALL, M. IMREGUN - *Mechanisms and Prediction Methods for Fan Blade Stall Flutter*. Journal of Propulsion and Power, 17(5), 1100-1108. Retrieved from https://arc.aiaa.org/doi/abs/10.2514/2.5850, September-October 2001.
- [57] M. VAHDATI, G. SIMPSON, M. IMREGUN - *Mechanisms for Wide-Chord Fan Blade Flutter*. Journal of Turbomachinery, 133(4), 2011.
- [58] M. VAHDATI, N. SMITH, F. ZHAO - *Influence of Intake on Fan Blade Flutter*. ASME Turbo Expo: Power for Land, Sea, and Air. Düsseldorf, Germany, 16-20 June 2015.
- [59] E. VAN DER WEIDE, A. K. GOPINATH, A. JAMESON - *Turbomachinery Applications with the Time Spectral Method*. 35<sup>th</sup> AIAA Fluid Dynamics Conference and Exhibit. Toronto, 6-9 Juin 2005.
- [60] J. M. VERDON - *Review of Unsteady Aerodynamic Methods for Turbomachinery Aeroelastic and Aeroacoustic Applications*. AIAA Journal, 31, 235-250, 1993.
- [61] S. WANG, S. LI, X. SONG - *Investigations on Static Aeroelastic Problems of Transonic Fans Based on Fluid-Structure Interaction Method*. Proceedings of the Institution of Mechanical Engineers, Part A: Journal of Power and Energy, 230(7), 685-695, September 2016.



**Alain Dugeai** graduated from the "Ecole Centrale de Paris" in 1985. He received a specialty degree in "Aerospace Mechanics" from the "Ecole Nationale de l'Aéronautique et de l'Espace" in Toulouse in 1986. Alain Dugeai has been working as a research engineer at ONERA's Structural Department in Chatillon, FRANCE since 1988. He has been involved in several development topics dealing with numerical aeroelasticity, such as: supersonic linearized numerical aeroelasticity methods, unstructured grid formulations for aeroelasticity, and mesh deformation techniques. He has been involved in the development of the aeroelastic module of ONERA's non-linear aerodynamic solver *elsA* since 2000, and was in charge of the development of numerical aeroelasticity and fluid-structure coupling methods for turbomachine and propeller applications. He is involved in several cooperation programs with industrial and academic partners, concerning civil aircraft and turbomachinery aeroelasticity, within both national and European collaboration contexts. He is now head of the Aeroelastic Modeling and Simulation unit (MSAE) of the Aerodynamics, Aeroelasticity and Acoustics Department (DAAA) of ONERA.



**Yann Mauffrey** is a research engineer in the Aeroelastic Modeling and Simulation unit (MSAE) of the Aerodynamics, Aeroelasticity and Acoustics Department (DAAA) of ONERA.



**Antoine Placzek** graduated from the mechanical engineering school Supmeca and obtained a Master's Degree from the University of La Rochelle. He received his PhD in Mechanics from the CNAM in 2009 and has since been working at Onera, where he is currently in charge of numerical developments for turbomachinery aeroelasticity.



**Simon Verley** is a scientist researcher in aeroelasticity of rotating bodies. He obtained his engineering diploma from ESTACA Paris in 2008 and his PhD in aerodynamics from the University of Orleans in 2012, on the topic of the evaluation of "Far-field" torque of a helicopter rotor during hover. Since then, he has been studying aeroelasticity of turbomachinery, CROR and helicopters. His main topics of research are the study of the whirl-flutter of CROR engines, the non-linear coupling between the *elsA* CFD software and the MSC Nastran CSM software and the coupling between *elsA* and the helicopter comprehensive code HOST.